HANDED AND POLARIZATION BEHAVIOR OF CORTICAL MICROTUBULES

A Thesis

Presented to the Faculty of the Graduate School

of Cornell University

in Partial Fulfillment of the Requirements for the Degree of

Master of Science

by

Xuan Shen

May 2013

ABSTRACT

The orientational alignment of cortical microtubule (CMT) arrays in interphase plant cells is crucial in determining the emerging anisotropy in cell expansion. Most models of the cortical array to date treat the interaction of two microtubule as one incident microtubule colliding with a barrier microtubule, with nucleation occurring both homogeneously in the cortical media, and along the length of existing microtubules. A key aspect of cell development not captured in these models is the differentiation of left- and right- handed macroscopic behavior, that can eventually lead to the development of chiral asymmetries at the tissue level. Here we propose plausible mechanisms for interactions within the restrictions of the existing experimental data that can explain certain experimentally observed macroscopic asymmetries for the polarization and precession of cortical microtubule arrays. To achieve polarization, we propose an linker protein that preferentially binds to and stabilizes copolar microtubules, this manifests in a different critical angle of entrainment. For precession of the microtubule array, we propose a chiral nucleation complex that preferentially nucleates on one side of existing microtubules. We verify the models with computer simulations of the cortical microbutules with 2-D periodic boundaries.

The polarization ordering of microtubule, much like the typical orientational ordering can be expressed as a scalar oder parameter that has an absolute value of 1 for fully ordered system and zero for completely disordered systems. But the nature of organization for systems with intermediate values of the order parameter is unclear and seems to shift as a function of system size. This raises the

question: is the observed order purely to the local interaction of microtubules, or do the finite size of system play a significant role. We address this question by extracting an additional parameter based on the time-domain histograms of the scalar order parameter, which allows us to clearly define if a system is ordered or disordered. Using this newly defined parameter, we find that the size of the system has a dramatic effect on both the orientational and polarization ordering of the CMT arrays, and as system size becomes larger the threshold ordering requires significantly higher rates of interaction between CMTs.

TABLE OF CONTENTS

LIST OF TABLES

LIST OF FIGURES

Chapter 1

Introduction

Microtubules are rigid structural macromolecules that form an integral part of the cellular cytoskeleton. These macromolecules are present in animal fungal and plant cells, serving dramatically different functions. As part of the cytoskeletal network, the microtubule is responsible of key cellular functions including mitosis, organelle positioning, and vesicle transport. Disruptions in the microtubule dynamics has been linked to diseases such as Alzheimer's and Parkinson's, as well as certain forms of cancer. The macromolecules are tubular proteins approximately $25\,nm$ in diameter, and varies in length up to $10^3 \mu m$. These microbutules can grow and shrink based on internal stochastic mechanisms and external stimuli.

As a structural macromolecule, microtubules often organize into large ordered structures inside of different organisms. In animals cells the microtubules form astral arrays centered around nucleation complexes called centrosomes; while in plants they form parallel arrays in the cortex (cytosolic side of the plasma membrane). Together, these microtubule arrays are the largest molecular structures found in nature.

A central question is how microtubules are able to organize into these large structures, specifically how the microscopic interaction between microtubules are parleyed into organization at a macroscopic scale. For this thesis we will examine how the orientational organization of cortical microtubules(CMTs) in plants arise from microscopic interactions, and how asymmetries in those interactions are translated to the macroscopic structures.

1.1 Microtubules

The molecular foundation of microtubules are polymers chains called protofilaments, composed of dimers of the proteins α-tubulin and β-tubulin , arranged in a hollow cylinder 25 nm in diameter. The microtubules are polarized macromolecules since all of the tubulin dimers are oriented in the same direction. The end with protofilaments terminating in a α-tubulin is designated as the $-$-end of the microtubule, while the end with terminal β-tubulin is designated as the $+$-end.

The growth of microtubules is highly dynamic with the plus end constantly switching between two distinct states of constant growth and rapid shrinkage. The transition between growth to shrinkage is termed *catastrophe*, while the opposite transition is termed *rescue*. This behavior of switching between multiple growth modes is called *dynamic instability*.

To model the behavior of CMTs in the context of dynamic instability, we will use a common model proposed by Mitchison and Kirschner [27] and described in partial differential equations by Dogterom and Leibler [13]. The model assume distinct characteristic time scales for catastrophe and rescue of the microtubule tips. This model predicts an exponentially decreasing length distribution, which is confirmed by experiments [22].

The growth properties of one end of the microtubule can be described by only four parameters: the growth and shrinkage velocities and the transition frequencies between the two states. These growth dynamics are emerges from the molecular properties of the tubulin subunits. In a growing microtubule, the tubulin dimers at the tip are associated with a GTP (guanosine triphosphate) molecule, which form a stabilizing cap that promotes polymerization. As the microtubule grow, the GTP associated with older parts of the microtubule are hydrolyses to form GDP

(guanosine diphosphate) which make the microtubule unstable. A catastrophe event occurs when the tubulin dimers at the tip of the microtubule experiences hydrolysis and is no long able to maintain the growth.

1.2 Functions of microtubules

As mentioned, organized microtubule structures are responsible for a variety of function in different cells. Here, we will discuss two particular examples in detail: the mitotic spindle during eukaryotic cell division; and cortical microtubule during cell elongation.

1.2.1 Mitotic spindle

Mitosis is a key step in the replication process of eukaryotic cells. During mitosis, two copies of the genetic material is transported to opposite ends of the mother cell so that one copy is retained by each daughter cell. The life-cycle of the cell is divided into several phases. The time between cell divisions, during which the cell grows by producing new proteins and cytosolic organelles. It is also during this phase, that DNA is replicated. During prophase, the genetic material in the cell condenses into chromosomes which contains indentical copies of the DNA of the mother cell. At the same time, astral arrays of cytosolic microtubules call mitotic spindel forms in the cell, originating from dense nucleation complexes called centrosomes. The microtubule attach to the different copies of the genetic material during metaphase, and the different copies are eventually pulled apart to opposite poles of the cell (in anaphase). After mitosis, the cytoplasm of the mother cell is divided through cytokinesis.

Mitosis of higher plantes such as *Arabidopsis thaliana* is significantly different

from the process stated above since they do not contain centrosomes. Prior to prophase, a thick band of microtubules and actin filaments form at the site of the future division. This structure is called the preprophase band.

1.2.2 Plant cortical microtubules

The cytoskeletal structure of plant cells differ greatly from their animal cell counterparts. Plant cells are surrounded by a rigid cell wall composed primarily of cellulose. To allow for anisotropic growth such as the unidirectional elongation of root and stem cells, a mechanism is required to direct cellulose deposition in the formation of new cell walls. A key feature of the cytoskeletal structure of the cell during elongation is the formation of large ordered microtubule arrays in the cortex of cell. The CMTs typically organize into parallel arrays where the orientation of the CMTs is perpendicular to the elongation direction of the cell.

Unlike the astral array found in animal cells, the CMTs in plant cells lack an obvious center to organize about, and are said to be *acentrosomal*. Hence the orientational organization observed for the CMT arrays are largely due to interaction between CMTs. Due to the emergence of ordering from interaction between the constituents of the system, this system is an intriguing one to study for statistical physics.

The interaction between CMTs are assumed to occur only when they are physically encounter each other during their growth. Since the CMTs are confined to grow in the two-dimensional space of the plant cortex, they will run into each other very frequently. The possible outcomes of these encounters (entrainment, crossover, and induced catastrophe) will be discussed in greater detail in the following chapters. Recent simulations studies of these same systems has confirmed that

these interactions are sufficient to produce the orientational ordering observed in the CMTs arrays. We will address some finer points in such as: the true nature of the transition between ordered and disordered arrays and its relationship to the size of the system and the effects of further symmetry breaking (polarization and precession) on the macroscopic behavior of the CMT array.

1.3 Brief chapter summaries

This thesis presents the basic mathematical model for simulating the interaction between plant CMTs with a focus on: connecting large scale polar and rotational asymmetries to molecular properties of microtubules; and identifying non-trivial phase transitions for the orientational and polar ordering of the CMT array; and

- Chapter 2: We present the mathematical models that govern the dynamics of individual CMTs, nucleation of CMTs in the cortex, and the interaction between them. Much of this material is based on the prevailing models used in the literature [2][15][10].

- Chapter 3: We describe specific design elements of the simulation we used, specifically: segmentation of the microtubules to increase efficiency during collision detection; and handling of interaction events when a growing microtubule is entrained along another microtubule.

- Chapter 4: We discuss the results of our simulations, without introducing additional symmetry breaking, and compare with existing studies. To better understand the nature of nematic ordering, we take the time-domain histogram of the order nematic order parameter and defines a fitting parameter that allows us to better define systems of intermediate nematic ordering. We

examine the behavior of the nematic fitting parameter as a function of system size. The orientational ordering show a decreased tendency to organize as the system size is increased, similar to a KosterlitzThouless transition.

- Chapter 5: We introduce a microscopic mechanism, in the form of an interaction bais between microtubules growing in different directions, that will allow the CMT arrays to become polarized — where the primary growth direction of the majority of CMTs are the same. After including the interaction biases into our simulations, we note a similar behavior to the nematic order as the system size is varied.

- Chapter 6: To simulate the experimentally observed rotation of the CMT array, We postulate additional microscopic bias in the nucleation frequency of microtubules along the length of existing CMTs, leading to a overall rotation of the organized CMT array.

- Chapter 7: Finally this chapter contains overall conclusions and a discussion of prospects of future studies.

Chapter 2

Modeling Of Plant Cortical Microtubules

2.1 Introduction

The cortical microtubules in plants were among the most prominent microtubule arrays in nature and were among the first microtubules to be directly observed Ledbetter and Porter [23] by electron microcopy. Formation and organization of these microtubule arrays have been the subject of recent experimental efforts (reviewed by Ehrhardt and Shaw [14], Wasteneys and Ambrose [36]) and simulation studies (by Allard et al. [2], Eren et al. [15], Deinum et al. [10]). Although there are no quantitative measures by which the models can be judged, they have all been able to reproduce various qualitative characteristics of the cortical arrays, most notably the emergence of nematic order, where the CMTs in the system mostly grow either parallel or antiparallel with each other.

Throughout this chapter, we will present the standard mathematical models used in our simulations to describe the dynamics of the cortical microtubules and the interactions between them. The model described in this chapter borrows heavily from [2, 15, 10]. A standard set of dynamic parameters will be presented, and used as a reference point to study the phase behavior of the CMT array as different parameters are varied.

2.2 Modeling of independent CMTs

Although the observed CMTs in the cortex appear to be highly dynamic with a constantly propagating center of mass, photobleaching experiments have shown

that the positions of individual tubulin subunits are fixed with respect to the plant cortex [31]. The observation of CMT translocation is completely due to the rapid transitions between different dynamical states at the plus-end — termed *dynamic instability* and the a net shrinkage at the minus-end [27].

Two state models have been pervasive in studies of microtubules dynamics and have been used to as measurement parameters by severals researchers of *Arabidopsis* root cells (Ishida et al. [20], Kawamura and Wasteneys [21]) and Tobacco BY2 (Dixit and Cyr [11], Vos et al. [35]). The wealth of experimental data for the various parameters makes the two state model the obvious choice for our simulations. But since there is not clear consense in the masurements of the various parameters, some of the parameters in our model will be variable to represent a wider range of dynamical behavior.

Tindemans et al. [34] and Deinum et al. [10] both adopted a two state model, where the dynamicity parameters are based on measurements of the plus-end dynamics measured by Vos et al. [35] and minus-end shrinkage measured by Shaw et al. [31]. Studies done by Allard et al. [2] and [15] used slightly different models to describe the dynamic instability at the plus end, each introducing new parameters into the model. Allard *et al.* used a three state model which incorporates an intermittent pause state in addition to growth and shrinkage. Eren *el al.* expands on the three state system by using a normal distribution of microtubule tip velocities, thus requiring two more parameters (the variances of the growth and shrinkage velocities) to depict the dynamics.

Our model for the dynamic instability of CMT tips follows Tindemans et al. [34] and [10]'s two state models with the same set of dynamic parameter. The dynamics of non-interacting CMTs is entirely described by a set of *five* dynamicity

Parameters	Symbol	Value	Description
PLUS-END			
Growth velocity	v_g^+	$0.08\,\mu m\,s^{-1}$	Constant rate of polymerization when the plus end is in the growth state
Shrink velocity	v_s^+	$0.16\,\mu m\,s^{-1}$	Constant rate of depolymerization in the shrink state
Catastrophe frequency	f_{gs}^+	$0.006\,s^{-1}$	Transition rate from growth to shrinking
Rescue frequency	f_{sg}^+	$0.007\,s^{-1}$	Transition rate from shrinking to growth
MINUS-END			
Growth velocity	v_s^-	$0.01\,\mu m\,s^{-1}$,	Constant rate of depolymerization at the mins-end
NUCLEATION			
Total nucleation rate	k_n	$0.001\,\mu m^{-2}s^{-1}$	Fixed total rate for both CMT-dependent and CMT-independent nucleation
CMT-dependent nucleation	p_d	0.75	Ratio of CMT nucleation that occurs on extant microtubules

Table 2.1: **Independent CMT dynamicity parameters**, overview of parameters that govern the behaviors of nointeracting CMTs. Most of the parameters are taken from Vos et al. [35].

parameters. The velocities of the plus end is fixed in each state at v_g^+ and v_s^+ where the subscripts (g) and (s) corresponds to the growth and shrinkage states respectively, and the transition rates between them is denoted by f_{gs}^+ and f_{sg}^+. The minus-end of the CMTs exhibit intermittent pauses between periods of slow depolymerization Shaw et al. [31]. Due to the strong depolymerization bias at the minus end, we do not expect the end to interact with other microtubules in the system and we can model the behavior with a single parameter v_s^-. The full list of parameters is given in Table 2.1.

2.3 Nucleation of CMTs

The lack of a centralized nucleation complex means that the nucleation of cortical microtubule is dispersed throughout the cortex. There is evidence that CMTs can be nucleated along the length of extant microtubules in the system in branching events Murata et al. [28] Wasteneys and Williamson [37], as well as the in the cell cortex itself Chan et al. [6] [37]. In recent simulation works Allard et al. [2] Eren et al. [15] and [10], both modes of CMT nucleation were included in the models. The rate of CMT nucleation is typically associated with the some fixed density of nucleation complexes in the cell cortex, resulting in a rate constant k_n of with units of $[time]^{-1}\,[length]^{-2}$ where the number of nucleation events is of the form shown in Equation 2.1

$$\text{[Rate Constant][Time][System Size]} \tag{2.1}$$

The simulations done by Allard et al. [2] assumes that the concentration of extant CMTs is rate limiting, and uses a separate rate constant with units $[time]^{-1}\,[length]^{-1}$ to describe the frequency of CMT-dependent nucleation. Other studies have chosen a fixed total nucleation rate and different models governing the percentage of each nucleation type. Eren et al. [15] uses a fixed percentage of CMT-dependent nucleation, while Deinum et al. [10] simulates a system with a fixed number of nucleation complexes, resulting in a rate of CMT-dependent nucleation that grows with system density.

Our simulations use the same fixed ratio model from Eren et al. [15], and a fixed fraction of 75 % for CMT-dependent nucleation is used since there are experimental evidence suggesting that the majority of nucleation occurring in the

system is CMT-dependent Murata et al. [28]. For the total nucleation rate, an estimated value of $k_n = 0.001\, s^{-1}\, \mu s^{-2}$ in accordance with the simulations by Deinum et al. [10], which produces organized arrays with our standard set of dynamicity parameters.

2.3.1 Angular distribution of CMT-dependent nucleation

The branching of microtubules follow an angular distribution that is strongly biased towards the plus-end of the mother microtubule Chan et al. [8]. In simulations bye Deinum, the CMT-dependent nucleation based on the observations by Chan et al. [8]: 31 % of branching microtubules follow the same direction of plus-end growth as the mother microtubule, another 31 % occurs on each side of the mother with distributions centered around $\pm 35°$ with respect to the plus-end of the mother, and the final 7 % is nucleated towards the minus-end of the mother. Allard's *et. al.* used a fixed angle of 40° for all the side-ways nucleation, which resulted in the evolution of unrealistic looking systems where all of the CMT concentration is focused in a few sparse bands. The simulations by Deinum et al. [10] also showed bands of high CMT concentration, which may be the result of a significant amount of CMT-dependent nucleation occurring parallel to the mother CMT.

The relative angles of CMT-dependent nucleation in our simulation are sampled from a uniform distribution centered at θ_b on each side of the mother microtubule (Figure 2.1). The exact value of $\theta_b = 25°$ represents the approximate center of the experimentally measured distribution from Chan et al. [8] when we include all of the nucleations occurring along the length of the mother CMT.

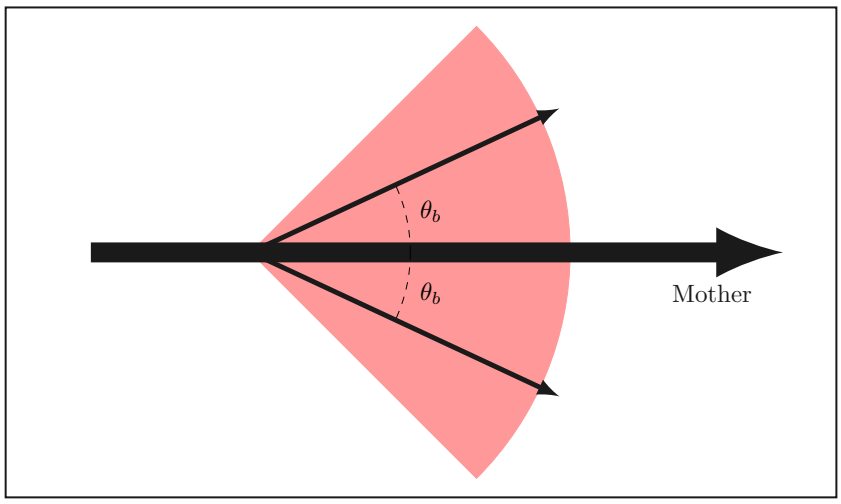

Figure 2.1: **Angular distribution of CMT-dependent nucleation**

2.4 CMT-CMT Interactions

Due to the dynamics of the cortical microtubules being confined entirely to the two dimensional space of the cell cortex and the relatively high density of CMTs in the system, encounters between the growing plus ends of the CMTs and the length of other CMTs in the system are very frequent. As the growing, "incident" CMT encounter another "barrier" microtubule, there are several different ways in which the interaction can be resolved. The incident microtubule may transition from a growing state to a shrinking state in a "catastrophe" event. It can also "cross over" the barrier microtubule and continue its growth on the other side or be "entrained" parallel to the barrier microtubule, depending largely on the angle of approach of the incident microtubule.

The orientation angle of each rigid piece of CMT is given by the relative orientation of their direction of plus-end growth to the [10] direction in the range $[-\pi, \pi)$. We define the angle of approach between the incident — θ_i and barrier —

θ_b CMTs as the relative difference in radians between their orientation directions, restricted to $\theta \in [-\pi, pi)$. For the our basic model, we assume that the situations are identical for CMT approaching from the *left* and *right* as well as*along* and *against* and plus end direction of the barrier. This four fold symmetry allows us to reduce the range of interaction angles to $\theta \in [0, \pi/2)$. At shallow angles of approach (θ closer to 0), the interaction outcome probability is dominated by entrainment, and at steep angle (θ closer to $\pi/2$) the other two interactions are much more probable. In this section, we will outline the model we have adopted for our simulations, and the molecular mechanism behind these simulations based reports by Allard et al. [1].

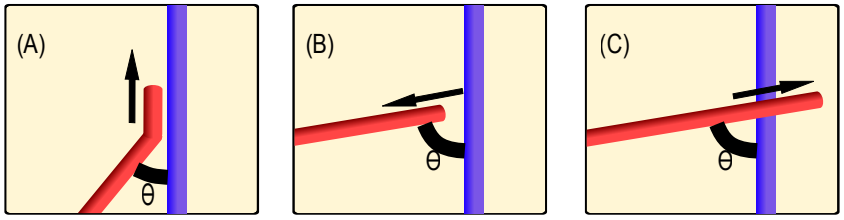

Figure 2.2: **Types of CMT interactions**: Three different types of CMT interactions found in our simulations. (A) Entrainment of incident microtubule at low angles of approach. (B) Catastrophe event, where the growing (*red*) CMT suddenly transitions to the shrinking state upon a collision with the barrier (*blue*) CMT. (C) Cross-over of the incident CMT over the barrier and continued growth on the other side.

2.4.1 Entrainment

The entrainment (some time referred to as "*zippering*") of the incident CMT has been reported by Ambrose and Wasteneys [3] and Dixit and Cyr [11]. While the molecular mechanism for entraiment is still unknown, observations have been made for molecular mechanism that govern both the amount of flexibility in a growing CMT tip Ambrose and Wasteneys [3] and the sustainment of bundling between CMTs by microtubule associating proteins Chan et al. [5]. Based on these observations, Allard et al. [1] proposed a mechanochemical model, suggesting that the flexible plus-ends of incident CMTs are progressively reoriented by associations with bundling proteins until they become parallel with the barrier at a fixed distance $\delta w = 35\,\text{nm}$ — the mean free spacing between CMTs taken from Chan et al. [5]. Predictions of Allard's model matches the experimentally observed data from Ambrose and Wasteneys [3], indicating that the lower energy cost of bending the plus-ends through shallower angles makes entrainment very likely at lower angles and almost prohibitive at high angles of approach.

Although detailed models of the CMT interaction resolution exists Allard et al. [1] [17], recent simulation works Allard et al. [2] Eren et al. [15] [10] have used piecewise constant probability distributions to determine the outcome of interactions in an effort to reduce computational cost.

In our model, a critical angle of $\theta = 40^\circ$ was chosen based on previous simulations efforts Eren et al. [15] Deinum et al. [10]. If the angle of approach is below the critical value, the resolution of the interaction will be entrainment with fixed probability. At angles higher than the critical value, the probability of entrainment is set to zero, so only cross-over and collision induced catastrophes are possible.

2.4.2 Collision and crossover

Aside from plus-end entrainment of microtubules, Ambrose and Wasteneys [3] reports two other types of CMT interaction outcomes prominent at high approach angles. The growing microtubules are observed to shift from the growth to shrinkage state upon encounter with another CMT which is termed collision-induced catastrophe (CIC), or continue to grow unimpeded by crossing-over the barrier microtubule. Models by Allard et al. [1] treated the microtubules is the cortex as thermally fluctuating rods bound to an infinitely rigid plasma membrane. Since the majority of CMT length in the system is anchored to the plasma membrane by CLASP proteins, all of the barrier CMTs are assumed to be fixed to the membrane and unable to undergo fluctuations.

Since newly grown tips of CMTs have relatively few associating CLASP anchors, they are relatively free to bend under thermal fluctuations. The stochastic nature of fluctuations dictates that a fixed percentage of growing plus ends, the deflection in the tip will be enough to clear the diameter of the barrier microtubule and cross over to the other side. For the rest of the CMT tips that do not cross over in Allard et al. [1], the resolution of the interaction will be either entraiment or catastrophe, with the probabilities determined by the entrainment model from 2.4.1.

In our piece-wise constant model, the probability of catastrophe is fixed at p_{cat} for interactions angles greater than θ_c. Experimental evidence for the probability of collision induced catastrophe varies wildly between species Dixit and Cyr [11] [38] and simulations by Allard et al. [2] have shown that induced catastrophes are no necessary for the formation of paraelle arrays. Due to the uncertainty and relative unimportance of the P_{cat} parameters, we choose an intermediate value of

$p_{cat} = 0.5$.

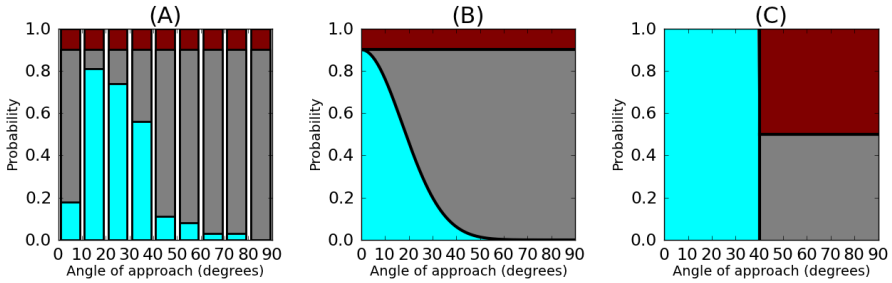

Figure 2.3: **Probability distributions of interactions**: Probability distributions of CMT interactions. (A) experimentally observed relative frequencies from Ambrose and Wasteneys [3] with a imposed fixed probability for collision-induced catastrophe at all angles. (B) Theoretical predictions of the probability distribution by Allard et al. [1]. (C) The simplified scheme used in our models with a critical angle of 40°.

2.4.3 Other interactions

Other less common modes of interaction between CMTs have been observed experimentally. Once a incident microtubule have crossed over a barrier, it may be severed at the cross-over point, most like by a katanin like agent. When the microtubules are in close proximity with one another, the same bundling proteins responsible for the reorientation during plus-end entrainment will be able to translocate the short pieces of CMT, this allows short minus-ends of entrainment microtubules to be moved with respect to the cell cortex and become entrained

with the barrier. The inclusion of cross-over severing has relatively little effect on the orientational behavior of CMT arrays Allard et al. [2], and translocation of minus-ends will have almost no effect since the persistent depolymerization at the minus end will remove any unbundled short minus-ends in a timely manner. Since these interactions have little to no effect on orientational organization of the CMT array, they are not considered in our simulation.

2.5 Boundary conditions

A typical plant cell is roughly cylindrical with a diameter of approximately $10\,\mu$m and a length measured between the anterior and posterior ends of about $100\,\mu$m. In the more recent set of literature on CMT simulations, the $80\,\mu\text{m} \times 80\,\mu\text{m}$ square system sizes in simulated by Deinum et al. [10] fall closest to this actual size. Other simulations have used periodic boundaries in the x-direction, and either a catastrophe-inducing Eren et al. [15] or reflective Allard et al. [2] y-boundary. We choose to focus on the process of CMT array orientation and not the orientation angle with respect to some external basis. Hence the y boundaries in our simulations are also given periodic boundary conditions. We do this in hopes of making our systems effectively infinite, but as we will see in Chapter 3, the geometry of organized CMT domains make finite size effects very difficult to eliminate.

Chapter 3

IMPLEMENTATION IN COMPUTER SIMULATIONS

We used *C++* programing language to conduct discrete time simulations of the behavior of cortical microtubule (CMT) arrays. The simulated behaviors include: then dynamic instability of CMT tips, CMT-independent and CMT-dependent nucleation, detecting the encounters between microtubules, and deciding the outcomes of those encounters. This chapter will outline some of the technical problems we've encountered while developing such a simulation and our methods to overcome these difficulties

3.1 Discrete time steps

All of the parameters in the mathematical model detailed in Chapter 2 describe a system under continous time evolution. To efficiently simulate the dynamics and interactions of many microtubules, we assumed that the occurrence of all spontaneous events in the system (i.e. nucleation, catastrophe and rescue) are approximated by Poisson statistics. The probability of an event occurring in an infinitesimal time step dt is given by $f\,dt$ where f is the mean frequency observed for that particular event. We can simulate the behavior of such processes with a discrete time-step Δt, so that the probability of the event occurring in one time-step is $f\,\Delta t$. This is valid as long as $f\,\Delta t \ll 1$, which makes the probability of multiple events occurring in the same time-step effectively zero. In the continuous limit as $\Delta t \to 0$, the discrete time model approximates a true Poisson process

and give a exponentially decaying waiting time between successive events for each process.

With our chosen discrete time-step of $\Delta t = 1\,sec$ we can verify the model against theoretical predictions of the two state dynamic instability system by Dogterom *et al.* Dogterom and Leibler [13]. The analytical model in Dogterom and Leibler [13] asserts that the critical parameter g given by determines whether the grow of the noninteracting microtubule is bounded or unbounded.

$$g = f_{sg}^{+}\left(v_{g}^{+} - v_{s}^{-}\right) - f_{gs}^{+}\left(v_{s}^{+} + v_{s}^{-}\right) \tag{3.1}$$

If $g < 0$ all any noninteracting microtubule will have a finite lifespan, and eventually completely depolymerize. However, if the set of dynamicity parameters are such that $g > 0$, the analytical model by Dogterom and Leibler [13] predicts a average polymerization rate of:

$$J = \frac{g}{f_{sg}^{+} + f_{sg}^{+}} \tag{3.2}$$

Since the changes in the system will happend on a much longer time scale than the standard one second time-step, we don't neet to continuously measure the system properties. From all of our simulation, a sampling period of $T_{sample} = 50\,sec$ will be used.

3.2 Segmentation of CMTs

The typical number of microtubules in our simulations, using a system size of $80\,\mu m \times 80\,\mu m$ and a the dynamicity parameters from Table 2.1, is around $10^3 \rightarrow 10^4$ individual microtubules. The high number total of individual microtubules creates a substantial speed restriction during the simulations, most noticeably

during the detection of collisions between microtubules, which is typically a $\mathcal{O}(N^2)$ process. To limit the number of collision detection calculations required at each time step o our system, we only check for possible collisions between the growing microtubule tips and CMTs segments that are within a small neighborhood of that tip. To achieve this, we subdivide the two-dimensional space of the cortex into a evenly spaced 30×30 square grid, where each square subsection is called a *sector* of the simulated space. Every microtubule in the system is partitioned into segments, each of which lies entirely within a sector. This type of segmentation allows us to only check for collisions in the blocks that contain the newest part of the incident microtubule after growth during the latest time stop. Aside from the segmentation of CMTs at sector boundaries, new segments are also created when the direction of plus-end growth is altered during entrainment events.

The segments themselves are stored in various linked lists, where the spatial information of each segment in the system is store in *nodes* and each node is connect to other nodes by memory references as part of a linked list used at different steps of the simulation Antonakos and Mansfield [4]. The primary list contains all of the segments in the system, with each segment sequentially connected with the other segment of the same microtubule, and new microtubules are added to the end of the list. Since each node of data in a linked list can only be accessed by traversing through other nodes, it is necessary to keep secondary lists that are subsets of the primary list to reduce the traversal time for specialized tasks like growing the time tips and checking for interactions within a sector of the system. An illustration of the different lists below can be found in Figure 3.1

- $\mathcal{S}$ — *List of all segments* : each segment of CMT that is in the system is represented by a node in this list. The nodes in this list are connected

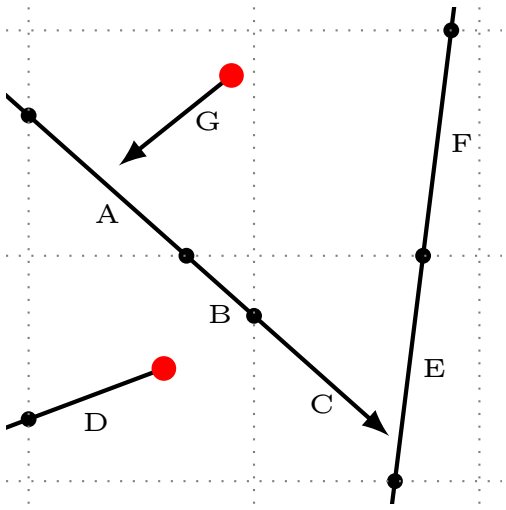

Figure 3.1: **Segmentation of microtubules in four sectors**. The dotted grid represents the boundaries of four neighboring sectors in the system and the arrows represent CMTs in the system pointing from the minus-end to plus-end. The segments are lettered (A) to (G), all belong to the list $\mathcal{S}$. The segments (C) and (G) both belong to the list of plus end segments $\mathcal{P}$, while the segments (D) and (G) belong to $\mathcal{M}$. The list of neighbors for the four sectors are:
$\mathcal{N}_{0,0} = (B, D)$; $\mathcal{N}_{0,1} = (C, E)$; $\mathcal{N}_{1,0} = (A, G)$; $\mathcal{N}_{1,1} = (F)$.

through computer memory references to sequentially adjacent segments on the same microtubule in both the plus and minus end directions. When each microtubule is nucleated in the system, it is assigned a incremental numerical index, the segments within a given CMT is ordered from the minus to the plus end and entire CMTs are order based on the numerical index by connecting the plus-end of an older CMT with the minus-end of the newer CMT.

- $\mathcal{P}$ — *List of plus-ends* : the plus-end terminating segment of all microtubules in the system have memory references to the other plus-ends which consti-

tutes a linked list only containing these segments. The ordering in this list follows the same numerical index as the primary list of all segments. By keeping the subset of plus-end segments in a separate linked list, we only need to access these segments when we compute the outcome of plus-end dynamic instability, thus dramatically reducing the traversal time needed.

- $\mathcal{M}$ — *List of minus-ends* : while the minus-ends segments are typically less dynamic than their plus-end counterparts, the implementation of the same type of linked list structure will still dramatically reduce the number of traversal need when computing the new positions of the minus ends after shrinking.

- $\mathcal{N}_{\alpha,\beta}$ — *List of all neighbors* : To reduce the number checks needed to detect interactions of CMTs in the system we keep all of the segments in each sector in a linked list where the segments are ordered chronologically based on when they were created within that particular sector. The indices α and β are both in the range $(0 \rightarrow 29)$, with $\alpha = 0$ and $\beta = 0$ at the bottom right corner of the system.

Since all of the segments in each sector can be found as part of linked list data structure, we only need to check for interaction in near-by sectors instead of the entire system. This dramatically decreases the number of calculations needed to determine if two CMTs will interact with one another, allowing for much after computing times. Assuming the mean length of CMTs in the system to be approximately $^1/_5$ the side length of the system — which will occupy about 6 sectors, the number of calculations required will be $\frac{6}{30\times30} \approx 0.6\%$ of the number needed for the naive method of simply checking each part in the system. The side lengths

of the sectors are still considerably greater than the distance that a microtubule can growth in one time step, both to restrict the number of sector that a growing tip can occupy and to limit the memory requirement for doing simulations. Thus the growing tip can cross boundaries at most twice during one time step — by growing out of one sector, across the corner of a second sector and ending inside of a third. We check for interactions in such situations by first checking in the sector containing the older part of the growing tip and move onto more recently occupied sectors if no interactions were detected.

3.3 Treatment of entrainment events

Recall that in our simplified model of CMT-CMT interaction, if the angle between the incident and barrier CMTs is less than the critical value θ_{end}, the incident microtubule will alter its direction of growth to be either parallel or antiparallel to the barrier. Since real CMTs are large macro-molecules of finite size and not infinitely thin rods, the entrained micortubule cannot occupy the same space as the barrier CMT. Gaillard et al. [16] showed that AtMAP65-5, a member of the Arabidopsis MAP65 family of proteins, simultaneously binds to two microtubules and promotes the formation of antiparallel microtubule arrays *in vitro*, with a uniform gap distance of approximately $24\,nm$. We note that the exact distance is likely not a key parameter for the orientational behavior of the CMT array, and other less undrestood MAPs with similar functions and varying sizes do exist. We elect to use a constant estimated bundling distance of $w = 30\,nm$ between entrained microtubule centers — including the $12\,nm$ radii of the entrained CMTs, which corresponds to a gap distance of only $\approx 8\,nm$. This was done so that the distance of microtubule plus-end growth $v_g\,dt = 80\,nm$ is not too large compared

with the bundling distance, reducing the lagging effect during interactions.

After an incident CMT segment determined to entrain along another CMT, we keep the length of newly grown CMT up to the point of intersection between the incident and barrier CMTs and initiate a new segment branching from the incident CMT at a point with perpendicular distance w to the barrier CMT. Illustrations of the entrainment interaction are shown in Figure 3.2.

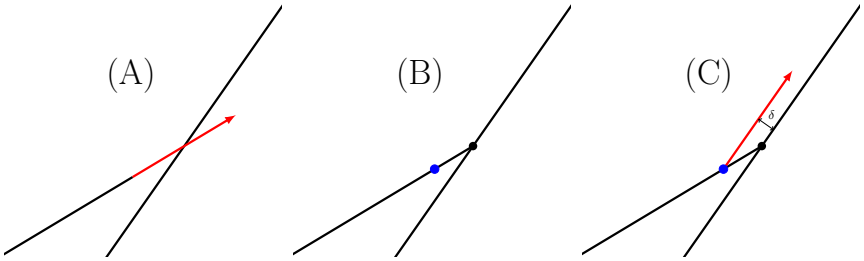

Figure 3.2: **Illustration of entrainment interactions**, showing the way our simulation deals with and entrainment event over two time-steps. (A) The plus end of a growing CMT encounters a barrier CMT, the red portion of the microtubule is the length added during the last growth step. (B) The incident microtubule is determined to entrain and a new segment of zero length is added before the point of intersection (at the *blue*point). (C) The newly added segment now grow parallel to the barrier at a universally fixed distance δ

.

Chapter 4

Orientational Ordering of CMT Arrays

Extracting useful information from the simulation of cortical microtubules is complicated by the fact that there is little agreement in the literature regarding the exact values of the parameters that describe the dynamicity of the individual microtubules. The standard set of parameters in our simulations have been presented in Chapter 2 and is closest to the set of parameters used by Deinum et al. [10]. In this chapter, we present the molecular mechanism for orientational (or nematic) organization, our method for measuring the degree of order, and changes in the order as the dynamicity parameter is varied.

4.1 Molecular mechanism

Recall that the primary modes of interaction between growing CMTs and existing lengths of CMTs in the system are: entrainment, induced-catastrophe and crossover. It is well known that these interactions, confined to the two dimensional space of the cortex is the key mechanism driving the self-organization of CMT arrays. Recent efforts by Allard et al. [2] Eren et al. [15] and Deinum et al. [10] in the simulation of CMT arrays have shed light on the effect of each type of interaction. Entrainment events, are the only mechanism present in the system that actively reorients microtubules over time, while the induced-catastrophes selectively stabilizes large bundles of co-aligned CMTs and removes the CMTs that are discordant to any emerging nematic order. This simple model is sufficient to explain the self-organization of CMTs, but provides no preference for the actual orientation of the resulting array.

The naive expectation, since we have chosen a periodic boundary conditions on all four sides of the simulation domain, is to have a uniformly distributed orientation of separately evolved systems. But as we will see in later sections — finite size effects, which are obviously present in the real system of CMT arrays, will have considerable influence on the orientation.

4.2 Measuring order

Since all of the individual microtubule segments in our simulation are rigid rods with a fixed direction and orientation, we can index each segment in the system by $\{i\}$, characterized by a length l_i and an angle θ_i. We adopt the tensorial double angle order parameter $\mathbf{S}_2$ used by Deinum et al. [10]:

$$\mathbf{S}_2 = \begin{pmatrix} \langle\cos(2\theta)\rangle_l & \langle\sin(2\theta)\rangle_l \\ \\ \langle\sin(2\theta)\rangle_l & -\langle\cos(2\theta)\rangle_l \end{pmatrix} \tag{4.1}$$

Where the subscript $\langle\mathcal{O}\rangle_l$ denotes the *length-weighted* average of an argument within the parenthesis. The length weighted average of a scalar value $\mathcal{O}$ given by:

$$\langle\mathcal{O}\rangle_l = \frac{\sum_i l_i \mathcal{O}_i}{\sum_i l_i} \tag{4.2}$$

The degree of orientational organization in a given system may be represented by the scalar order parameter:

$$S_2 = \sqrt{\langle\cos(2\theta)\rangle_l^2 + \langle\sin(2\theta)\rangle_l^2} \tag{4.3}$$

For completely organized systems where all of the CMTs are either parallel or antiparallel to each other, S_2 attains the maximal value of 1; and for completely

discordant system, S_2 approaches the minimal value of 0. This measure of the orientational order ignores the polarization of CMT's in the array, additional order parameters that take the polarization into consideration will be considered in Chapter 5.

We aslo adopt Deinum et al. [10]'s definition of the net orientation angle Θ used to parameterize the unit eigenvector $\mathbf{n} = (\cos\Theta, \sin\Theta)$ whose magnitude is the order parameter S_2. The preferential angle can be extracted from the S_2 order parameter with:

$$\tan\Theta = \frac{\langle\sin(2\theta)\rangle_l}{\langle\cos(2\theta)\rangle_l + S_2} \tag{4.4}$$

This awkward expression is necessary because if we want to find the orientation of the CMT array up to the polarization, the value of Θ must span a range of size π — specifically the range $[-\pi/2, \pi/2)$. Hence the left side must be a trigonometric function of only Θ with no higher multiples. However, since we want to remove the dependence on CMT polarity, the right side must consist of ensemble averages of functions of 2θ, which is equal for θ and $\theta + \pi$, where θ is orientation angle of individual CMT segments in the range $[-\pi, \pi)$.

4.3 Handling large parameter spaces

Since there is no consensus in the measurements of dynamicity parameters and they change dramatically over the life-cycle of the cell [35], we have to examine the organizational behavior of the CMT array at different points in the parameter space to understand the conditions required for orientational organization. Due to the large dimensionality of the parameter space in our simulations (more than 15 independent parameters), we cannot hope to systematically explore each di-

mension due to the high cost of computation. The best we can hope to do is to identify some key parameters that control important characteristics of the CMTs in the system and observe how the organization changes with respect to these parameters. Following the example of Shi and Ma [32], we restrict ourselves to two control parameters that each guide one aspect of CMT dynamicity. The two control parameters for CMT dynamics we will focus on are the catastrophe frequency f_{gs}^{+} which determines the growth behavior of individual CMTs and the nucleation rate k_n which indirectly affects the overall density of microtubules in the system. The two parameters we have chosen to vary have been difficult to evaluate experimentally, making them a likely candidate for the small discrepancies in the results of past simulation studies.

4.4 Nematic phases

The combination of computational and theoretical studies were conducted by Shi and Ma [32] to better understand the phase behavior of CMT arrays. The model in these studies used a more complex system of rate equations to describe the dynamicity of the CMTs in the system. However, the only form of CMT-CMT interactions present in the model were steric interactions, where the incident microtubule simply stalled when it encounters another segment of CMT effectively increasing the likelihood of catastrophes. Shi and Ma [32] observed three distinct phases as the dynamicity and the overall density of CMTs are varied: an *isotropic* phase with discordant microtubules, a highly ordered *nematic I* phases with long microtubules and a weakly ordered *nematic II* phase with short microtubules. The general phase behavior of the simulated system, followed the mean-field predictions detailed in the same report.

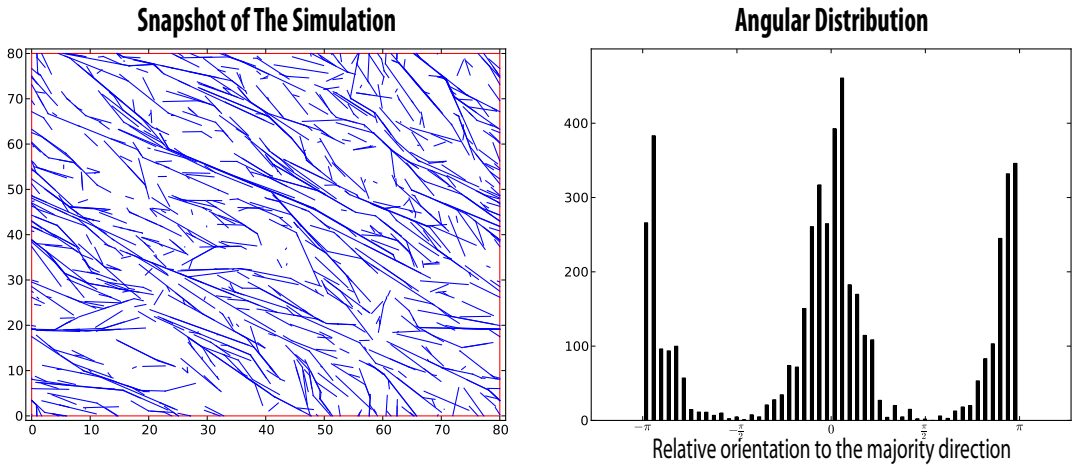

Figure 4.1: **Snapshot of the standard system** — with side length $L = 80\,\mu m$ and $f_{gs}^{+} = 0.006$, with the angular distribution of the CMT lengths at the same point of the simulation.

The angular distribution is shifted so that array orientation angle Θ corresponds to the origin.

The two control parameters used in the study of Shi and Ma [32] were:

- k_{gt} — the plus-end GTP-state growth rate, which controls how fast a growing plus-end is growing. While the parameter v_g^+ in our simulations serves as a good analogue to k_{gt}, the combined dynamic behavior of the plus end is also easily affected by changing our standard control parameter f_{gs}^{+} (the spontaneous rate of catastrophe)

- ρ — the microtubule number density. The microtubules simulated by Shi and Ma consists of a fixed number of small segments that can be in solution or bound to a long CMT polymer. Our simulations assumes a large quantity of tubulin subunits from the bulk of the cell cytosol which modulates the density of tubulin in the cortex. Thus, we do not have a strictly analogous

control quantity. We can simulates a change tubulin density by altering the total nucleation rate (k_n) of CMTs in the system.

For the systems with more complicated interactions (similar to those we have simulated), attempts at reconciling mean-field predictions and simulated results have been less successful [34]. These systems typically have less extreme S_2 values than the systems with only steric interactions. While the systems studied by Shi and Ma had clearly distinguishable organized and disorganized states, the more intermediate values and larger fluctuations in the S_2 order parameter makes it difficult to determine whether a given system, with the inclusion of complex CMT-CMT interactions and branch-form nucleation, is in the ordered phase.

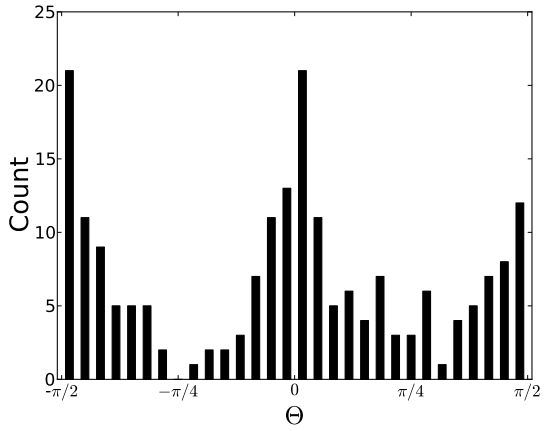

Figure 4.2: **Angular histogram of final array orientation** for 200 randomly seeded systems with the same set of dynamic parameter. Note that the distribution is weakly centered about 0 and $\pm\frac{\pi}{2}$, evidence of large domains interacting with itself across periodic boundary conditions.

The snapshot of a system with our standard parameter set and angular distributions of the snapshot are shown in Figure 4.1. Although the snapshots of the

system can be used to indicate the degree of order in the cases of very high or very low organization, they are insufficient in distinguishing the states with intermediate S_2 values. The method for analyzing these systems will be detailed in the next section.

Although we have chosen the periodic boundary conditions specifically to remove any external influence on the orientation of the CMT array, the finite size of the system still allows for the CMT array to preferentially align along the vertical and horizontal directions, as well as the diagonal as shown in Figure 4.2. This is primary due to the growing organized CMT domain interacting with itself across the periodic boundaries. The presence of this weak angular preference will have some effect on the precession of the CMT array (discussed in Chapter 6).

4.5 Phase transitions

A key point in our study of cortical microtubule arrays is to gain a better understanding of the of fundamental differences between the organized and discordant phases. This necessitates a more thorough study of transition between these phases. Since our system is not truly infinite, we expect finite-size effects to play a role in behavior of the transition.

Due to the lack of reorienting interactions in the systems described by Shi and Ma [32], the transition between the isotropic and highly nematic state are abrupt — showing a discrete jump in the order parameter with a marked *bistablity* where the ordered and disordered regimes overlap. Studies by Deinum et al. [10] showed that if shallow angle entrainment and CMT-dependent nucleation are included in the simulation, the same transition is sharp but clearly continuous. And if forward biases CMT-dependent nucleation is integrated into the simulations, the

transitions becomes much smoother.

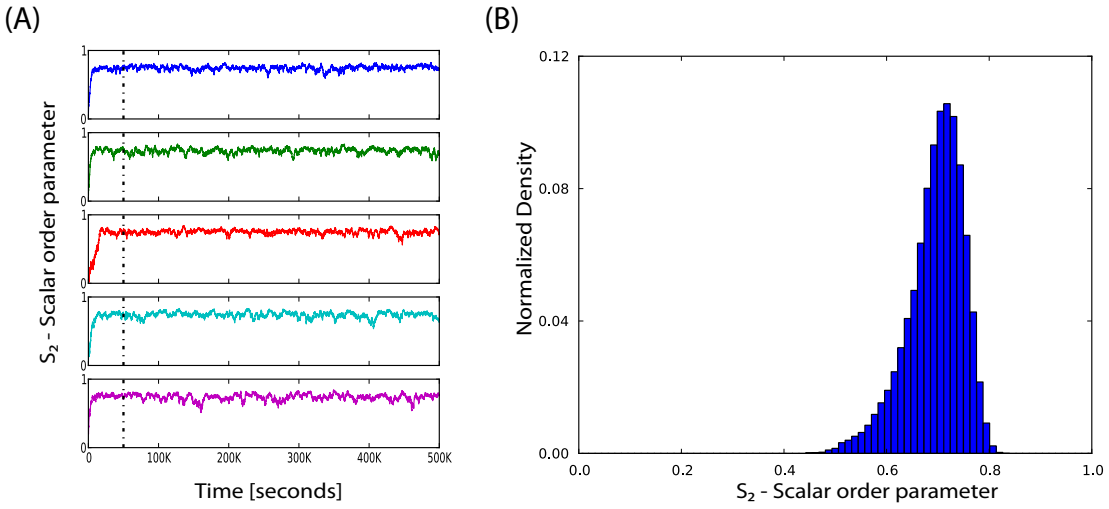

Figure 4.3: S_2 **Order parameter time-series and distributions** (A) Time-series of the un-corrected scalar order parameter for our standard system — as described in Table 2.1 — from five independent simulations. The dotted lines mark the initialization time we allow for the system to reach a steady state, the S_2 values during the initialization time are not tabulated in the final distribution. (B) the normalized density distribution of the S_2 order parameter from all five runs, after correcting for the effect of angular degree of freedom.

Our simulations closely resembles the systems used by Deinum et al. [10] and produces similar results. The transition in the orientational order appears sharp for systems without CMT-dependent orientation, but lacks the sudden transition and bistability observed by Shi and Ma [32]. For the systems with strongly forward biased CMT-dependent nucleation, we observe a similar broadening of the transitional range.

To better identify the transition between the ordered and disordered phases, we

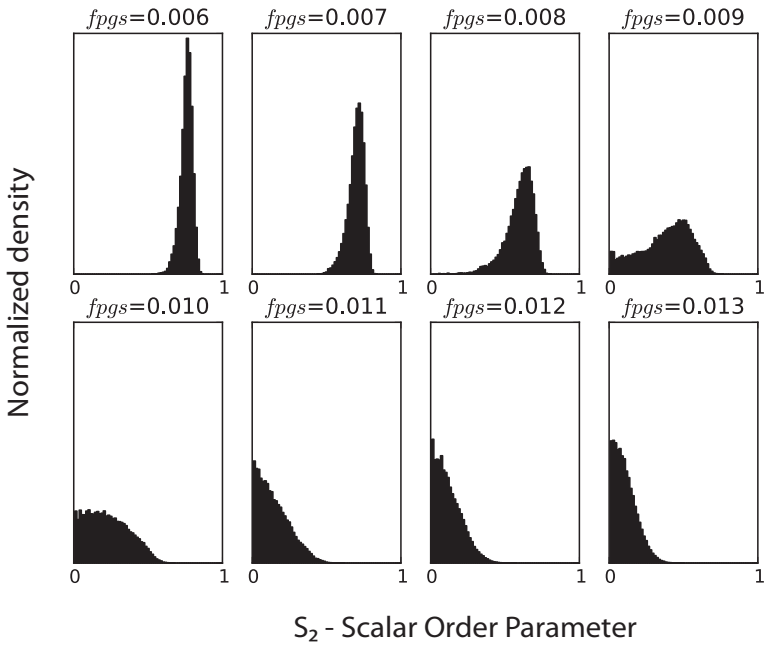

Figure 4.4: **Ordered-Disordered phase transition of the standard system with variable catastrophe rates.** The series of histograms show how the normalized density function changes as the spontaneous catastrophe rate is increased. The distribution goes from having a clear non-zero maxima in $f_{gs}^{+} = 0.009$, to having a clear maxima at zero in $f_{gs}^{+} = 0.011$.

examined the distributions of S_2 scalar value for different sets of control parameters. The S_2 values are sampled from the simulations at an interval of 50 time-steps, over 5 independent runs to ensure that the distribution is not affected by the time history of the system. Note that by taking the distribution in the time domain, we have made the assumption of no long term memory in the development of the CMT array. This assumption is corroborated by the fact that a small set of five randomly seeded simulations produces a distribution that is sufficiently smooth with one clear peak.

Since the order parameter S_2 corresponds to a orientation vector, the extra angular degree of freedom will scale the density of S_2 values as the magnitude is increased. The effective scaling is linear in the same way that a small ring of small width dr has an area of $2\pi \cdot r \cdot dr$ that is linearly dependent on the radius. To correct the fictitious bias towards larger S_2 values, we recorded each measurement in one of 40 bin in the range $(0, 1)$ and divided the counts in each bin by the value at the midpoint. The correct data is then normalized to give an approximate distribution of S_2 scalar order parameters that is independent of orientation. The time-series and resulting normalized distributions are shown in Figure 4.3.

The process can be repeated for a range of control parameters. For a fixed nucleation rate of $k_n = 0.001$ we varied the spontaneous catastrophe frequency f_{gs}^{+} from 0.006 to 0.013 in increments of 0.01 and recorded the same kind of time-domain histograms. While the transition in the S_2 value appears smooth across this range, the histograms allows us to identify the organized states as having a local maxima in the histogram at a nonzero value, and the disordered states as having a local maxima at the origin. The transition point for this particular set of simulations, with $k_n = 0.001$ and a system size of 80×80, the transition happens between the spontaneous catastrophe rates of $f_{gs}^{+} = 0.009$ and $f_{gs}^{+} = 0.010$.

Although the systems with periodic boundaries are clear capable of developing global order, we cannot determine whether the system of CMTs is capable establishing global order as the system size is increased. Determining the system sized dependence of the phase transition is crucial in determining the nature of the ordered and disordered phase.

4.6 System size dependence of phase transitions

Since we cannot simulate cortical microtubules in a system of infinite size, we can only hope to infer the behavior of the infinite system from simulations of finite systems. To do this, we examine the distributions of the S_2 scalar order parameter for $L \times L$ systems of three different sizes. In addition to the $L = 80\,\mu m$ systems we simulated in the previous section, we examined systems with $L = 40\,\mu m$ and $L = 120\,\mu m$ while fixing all other dynamical parameters. The resulting distributions and their dependence on the spontaneous catastrophe rate f_{gs}^{+} is shown in Figure 4.5. For the smallest systems ($L = 40\,\mu m$), the corrected S_2 values show relatively broad distributions for all values of the spontaneous catastrophe rate. The transition point for the $L = 40\,\mu m$ system — where the distribution changes from having a local minima at $S_2 = 0$ to having a local maxima — occurs between $f_{gs}^{+} = 0.011$ and $f_{gs}^{+} = 0.013$. As the size of the system is increased to $L = 80\,\mu m$ and $L = 120\,\mu m$, the transition shifts to $f_{gs}^{+} = 0.009 \rightarrow 0.011$ and $f_{gs}^{+} = 0.009 \rightarrow 0.010$ respectively. For the highly ordered systems ($f_{gs}^{+} = 0.006$ and $f_{gs}^{+} = 0.007$), the peaks of the distribution shifts to lower S_2 values, indicating that as the system size is increased, the degree of orientational organization will gradually decrease.

The likely explanation of the decreasing orientational organization for larger systems is that the systems which appear organized in our finite sized simulations are actually quasi-ordered states where the orientation correlation functions decays slowly as a power law, which varies with increasing displacement. This situation is very similar to the one encountered in the equilibrium 2 dimensional XY-model, where classical spin vectors of unit length are placed at regular lattice sites. Mermin and Wagner [26] showed that no conventional phase transition occurs in the infinite

2D XY-model, but there is a different kind of transition: the Kosterlitz-Thouless transition where with two distinct phases:

- A low-temperature, quasi-ordered phase, where most spins are locally aligned but the correlation-function decays with a power law. The local average of the spin vector varies continuously as a function of T or other parameters. The local orientation of the system lose correlation at long distance, but no free vortex is formed.

- An high-temperature, disordered phase, where the correlation-function decays exponentially as a function of distance. This is due to the formation of topological excitations in the form of vortices in the system. The vortices effectively break the correlations of the spins.

The critical transition temperature (threshold for free vortex formation), has been computed by Olsson [30] for the 2D XY-model with periodic boundary conditions. However, for our model of cortical microtubules, simulating systems larger than $120\,\mu m \times 120\,\mu m$ is computationally costly, and the exact value of the critical transition point has little significance since the dynamicity parameters are not well known and can be changed by the cell during development. What should be noted however is the physical size of the cell directly affects the degree of orientational order in the CMT array.

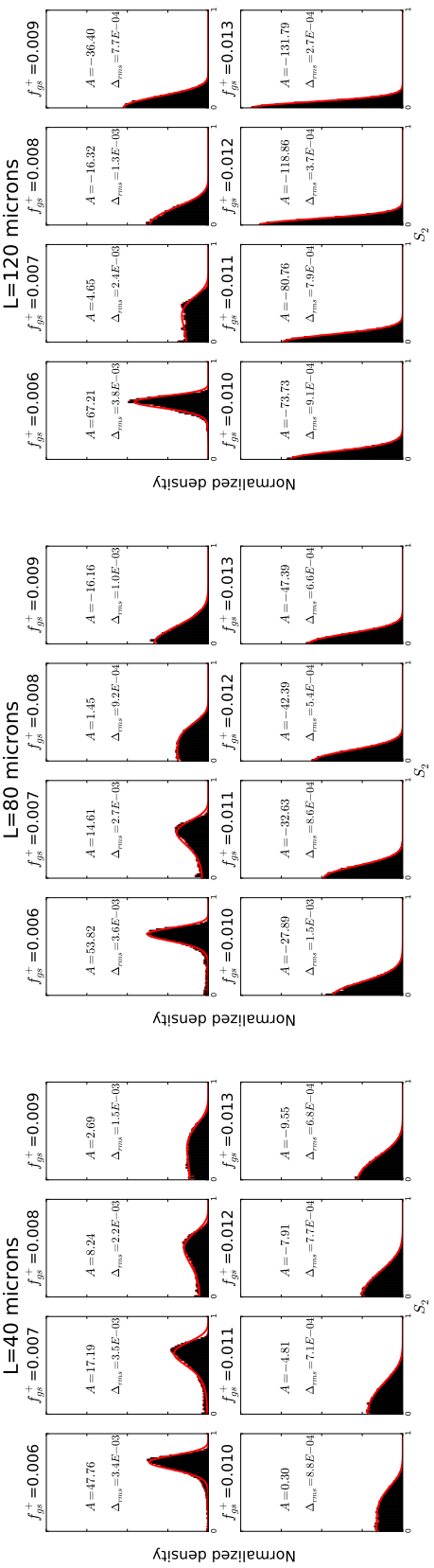

Figure 4.5: **Nematic order distributions at different system sizes.** The series of distributions showing the nematic phase transition of the standard system ($L = 80\,\mu m$)is shown in the middle pannel. The simulations are repeated for systems of size $40\,\mu m \times 40\,\mu m$ and $120\,\mu m \times 120\mu m$. As the system size increases, the normalized densities of the S2 scalar shifts closer to the origin. The distributions are fitted to quartic exponentials (shown in red)of the form $C\exp(Ax^2 + Bx^4)$, and the fitting parameter A is shown on each subplot. The root-mean-square difference between the data and fitting curve is given as Δ_{rms}.

We can distinguish between ordered and disordered systems at each system size by whether the distribution of S_2 values has a local maxima or minima at $S_2 = 0$. This is accomplished by fitting the distributions to a quartic exponential of the form:

$$f(x) = C \exp(Ax^2 + Bx^4) \tag{4.5}$$

Since the second derivative of the curve at the origin is given by $2AC$, a positive values of A indicates a minima at $S_2 = 0$, while negative values indicate a maxima. The curvature of the fitted function at $S_2 = 0$ is given by the parameter A and shown in Figure 4.6 for each system size. The dependence of the transition on the total nucleation frequency can also be examined by repeating the fitting process for difference values of k_n. The results are presented in Figure 4.7.

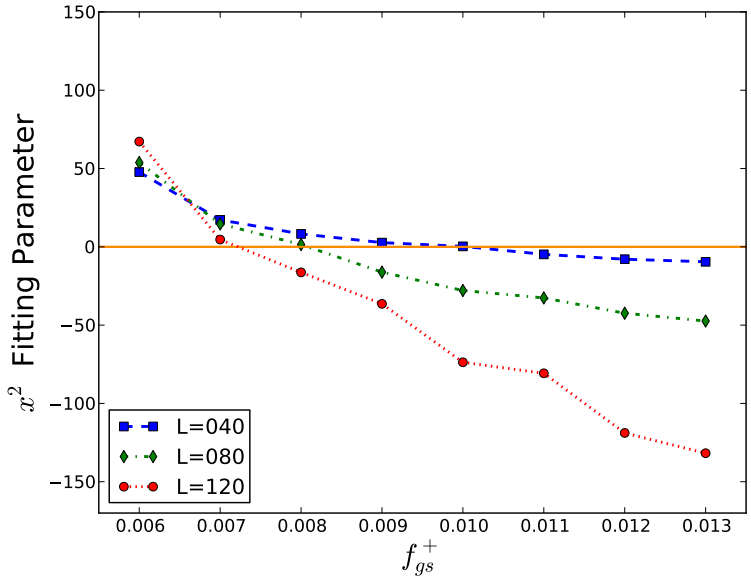

Figure 4.6: **Curvature of the nematic fitting function.** The fitting parameter A is plotted against the control parameter f_{gs}^{+} for systems of size $L = 40\,\mu m$, $L = 80\,\mu m$, and $L = 120\,\mu m$

The exact transition point remains difficult to identify, since the fitting of the quadratic exponentials is much better for the histograms centered at zero (negative A) than those that attain a maximum at a non-zero value (positive A). We can identify the transition point as the point where $A = 0$. The trend of decreasing transition values on the f_{gs}^{+} axis as a function of system size is clear. The system is biased towards the disordered state as the system size is increased, matching the expected behavior of a Kosterlitz-Thouless type transition.

In Figure 4.7 we plotted the fitting parameter A for a series of systems with different CMT dynamicity — controlled by changing the spontaneous catastrophe f_{gs}^{+} and the nucleation rate k_n, and system sizes. The data we have collected clearly indicates a number of trends:

- Fitting parameter A decrease as the spontaneous catastrophe rate is increase, since the shorter microtubule lifetimes do not allow for the CMT-CMT interaction to selectively stabilized the microtubules in a majority direction.

- For a fixed nucleation rate k_n, the transition point shifts to lower values of the spontaneous catastrophe rate f_{gs}^{+} at larger system sizes. Thus the disordered phase occupies more of the k_n-f_{gs}^{+} phase space in larger systems.

- As the nucleation rate k_n increases, the transition of the fitting parameter A becomes sharper and the transition point tend shift to higher values of f_{gs}^{+} especially for the larger systems.

Moreover, for the set of simulations we have performed, we have a roughly defined range for the critical value of f_{gs}^{+} at the transition points, shown in Table 4.1.

Nucleation Rate k_n	Critical f_{gs}^{+}
0.0005	$0.0068 \sim 0.0090$
0.0001	$0.0072 \sim 0.0100$
0.00015	$0.0076 \sim 0.0102$

Table 4.1: **Range of nematic transition values** of the control parameter f_{gs}^{+} for simulated systems with different rates of CMT nucleation (given by the control parameter k_n). The range is taken as the approximate range of transitional f_{gs}^{+} values between the systems with $L = 40\,\mu m$ and $L = 120\,\mu m$.

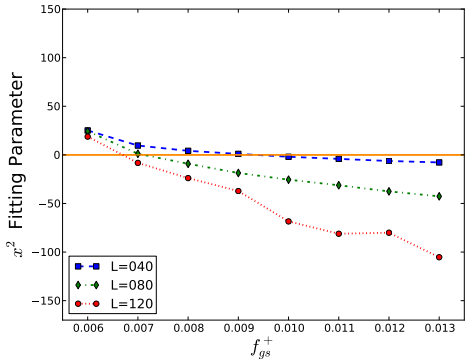

(a) $k_n = 0.0005$

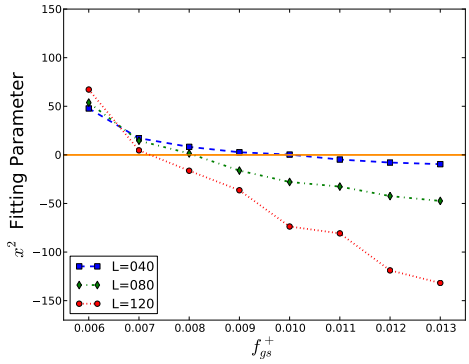

(b) $k_n = 0.001$ (reference system)

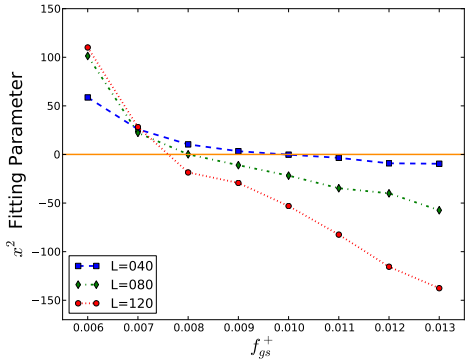

(c) $k_n = 0.0015$

Figure 4.7: **Dependence of the nematic transition on nucleation rate.** Simulations are repeat at $k_n = 0.0005$ and $k_n = 0.0015$ and the resulting distributions of the corrected S_2 order parameter are fitted to same functional form (Equation 4.5). The fitting parameter A is plotted against the control parameter f_{gs}^+ for systems of size $L = 40\,\mu m$, $L = 80\,\mu m$, and $L = 120\,\mu m$

Chapter 5

Polarization of CMT arrays

In the previous chapter, we have seen how the collective behavior of the cortical microtubule interactions leads to the nematic ordering of the population of CMTs in the system into larger organized arrays. While the nematic order accounts for the orientational ordering of the CMTs in the system, the polarization of the CMTs have been explicitly neglected (i.e. the definition of the order parameter only uses the double angle so that antipolar segments with orientations θ and $\theta + \pi$ are identical in the computation [Eq. 4.3]). Since there is no external influence on CMT polarity, global array polarization must arise from asymmetry in the relative polarization of interacting CMTs.

During the formation of organized CMT arrays, high degrees of global polarization were observed by Dixit et al. [12] and Chan et al. [7] experimentally. On the simulation side, Eren et al. [15] reported as much as 80 % of the CMTs in the system polarizing along the majority direction. A related phenomenon that can help explain the global array polarization is the selective stabilization of CMTs in the majority direction. The selective stabilization of majority direction CMTs was observed in [12] as CMT tips tend to grow in the majority direction for a longer time compared to the minority direction. The experimental studies also observed that the microtubules arrays are not biased to be polarized in any externally defined direction. Hence, the polarization must be caused by interaction between CMTs that selectively stabilize CMTs growing in the same direction.

In addition to the selective stabilization of co-polar CMTs, the strongly forward biased CMT-dependent nucleation has also been linked with establishing polar

order in the array [15]. We speculate that the forward bias in CMT-dependent nucleation only serves to increase the magnitude of the fluctuations in a system that is not really capable maintaining any degree of sustained polarization order.

5.1 Molecular mechanism

Although there is abundant evidence of plus end entrainment in growing cortical microtubules [31, 11, 3], little is known regarding the actual molecular mechanism that produces this phenomena. CMT-dependent nucleation was observed to have a strong nucleation bias such that new CMTs are nucleated more frequently along the +-end direction by Chan et al. [8], and the forward bias is postulated in the same report to cause an overall array polarity. The simulations in [15] showed that the inclusion of forward biased CMT-nucleation was able to produce mostly polarized systems, but our simulations (discussed later in this section) showed that the CMT-dependent nucleation alone is not able to produce a sustained polarization of the CMT array system.

Gaillard et al. [16] showed that certain microtubule associating proteins (MAPs), namely those in the MAP65 family, are likely to be responsible for the bundling of CMTs after the incident microtubule has already entrained. A mechanism proposed by Allard et al. [1] calls for the treatment of the MAPs as stiff Hookean springs which exert force along the length of the interacting CMTs and bends the incident CMT to bo parallel with the barrier. Allard's model was successful in predicting the preference for entrainment at shallow angles of interaction. However, due to the ambiguity in the polarization of the barrier microtubule (experiments typically do not distinguish the polarity of barrier microtubule), Allard's model considered the interactions to be identical regardless of whether the incident CMT

grows along or against the polarization of the barrier.

In addition to the nucleation bias evident in the real system, we propose a molecular mechanism for polar interaction bias based on possible asymmetries of bundling proteins similar to those found in the MAP65 family. Observations by Gaillard et al. [16] showed that the presence of specific MAPs (AtMAP65-5) can promote the formation of anti-parallel arrays *in vitro*. This suggests that the bundling proteins can preferentially bind to and/or stabilize antiparallel CMTs. If the MAPs can somehow distinguish the polarization of microtubules they bind to, then it is reasonable to assume the existence of an undiscovered MAP that selectively binds parallel CMTs. Within Allard's picture of the entrainment interaction, this selective binding will produce an higher probability of entrainment if entrained CMT and the barrier are polarized in the same direction, and a lower probability if they are polarized in opposite directions. In the context of our simulations, this bias can be reproduced by breaking the θ_c critical angle of entrainment into two separate parameters:

- θ_{along} — the critical entrainment angle for co-polar microtubule encounters.
- $\theta_{against}$ — the critical entrainment angle for anti-polar microtubules encounters.

5.2 Measuring polarization

All of the simulation studies to date have demonstrated the relationship between the interactions of the individual CMTs and the formation of nematically ordered arrays that span the entire system, but little has been done to model the development of polar arrays. Eren et al. [15] demonstrated polarity in a small number of

systems with the only forward biased CMT-dependent nucleation. However, these observations were only made for a few snapshots of the simulated systems and do not answer whether the polarizations are sustained as the systems continued to evolve. Our studies show that the CMT-dependent nucleation is insufficient to produce a persistent polarization in the system, and collision bias, by distinguishing between entrainment of co-polar and anti-polar microtubules, is sufficient to produce a sustained polarized array.

Measurements of the degree of polarization in the system is given by a projection of the vectorial order parameter $\mathbf{S}_1$ onto the unit vector in the direction of the orientation angle $\hat{\mathbf{n}} = (\cos\Theta, \sin\Theta)$, where $\mathbf{S}_1$ is the length weighted averages of the CMT segments and the angle Θ defined by Equation 4.4:

$$\mathbf{S_1} = (\langle\cos\theta\rangle_l, \langle\sin\theta\rangle_l) \tag{5.1}$$

Hence the order parameter is a scalar value given by:

$$P = \mathbf{S_1} \cdot \hat{\mathbf{n}} = \langle\cos\theta\rangle_l \cos\Theta + \langle\sin\theta\rangle_l \sin\Theta \tag{5.2}$$

We define the positive polarity for CMTs in the system to coincide with the direction given by the organized array angle Θ. Since the angle Θ is defined in the range $\left[-\frac{\pi}{2}, \frac{\pi}{2}\right)$, the positive polarity will always coincide with a vector whose orientation angle is in the range $\left[-\frac{\pi}{2}, \frac{\pi}{2}\right)$. We can visualize the polarization of the microtubule array by assigning different colors to the microtubule segments bases on sign of the projection onto $\hat{\mathbf{n}}$. Examples of polarized and unpolarized systems with similar dynamical parameters are shown in Figure 5.1. The blue microtubules have a positive projection component on the orientation vector $\hat{\mathbf{n}}$ and the red microtubules have a negative component.

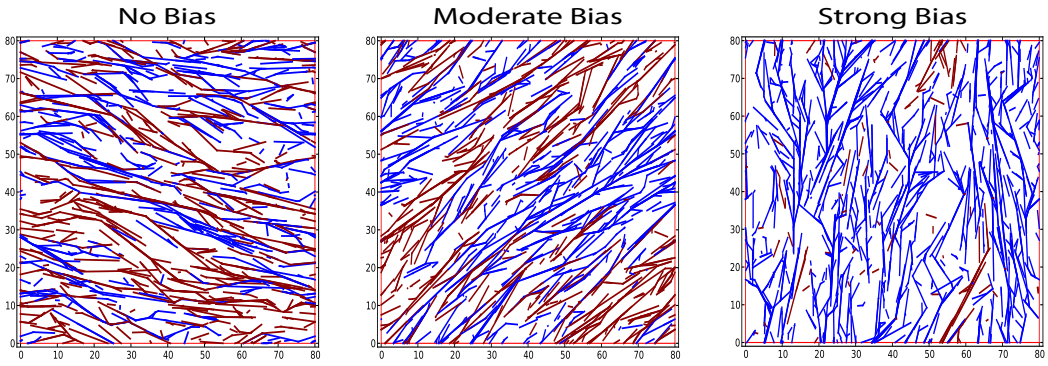

Figure 5.1: **Snapshots of color coded systems**, at various degrees of polarization induced by interaction bias. The system with no interaction bias has θ_{along} and $\theta_{against}$ both equal to 40°. The system with moderate bias has $\theta_{along} = 58°$ and $\theta_{against} = 22°$. And the system with strong bias has $\theta_{along} = 70°$ and $\theta_{against} = 10°$

In the systems with no polarizing interaction bias, small regions of uniform polarity can still form due to the strong forward bias in branch-form nucleation. Since the system has well established nematic order, the microtubules are mostly oriented along the orientation vector parallel to $\pm\hat{\mathbf{n}}$. The lack of interaction bias allows for oppositely polarized regions to penetrate into with each other, effectively mixing the microtubules with opposing polarities. As the interaction bias is increased, the neighborhoods of definite polarity are less capable of mixing with the opposite polarity, so the polarized regions will increase in size. As the polarization bias is increased even more, one region of definite polarity will dominate the entire system, as shown in Figure 5.1.

5.3 Polarization Phases

In the report by Eren et al. [15], simulated systems with branch-form nucleation had a much higher frequency of being observed in a polarized state. However, there was no thorough examination of how well the polarity in a given system correlates as the system continues to evolve in time. We use the same machinery developed in the previous chapter to study the phase behavior of the polarization: taking the time-series and distributions of the polarization and examine how they depend on the system size.

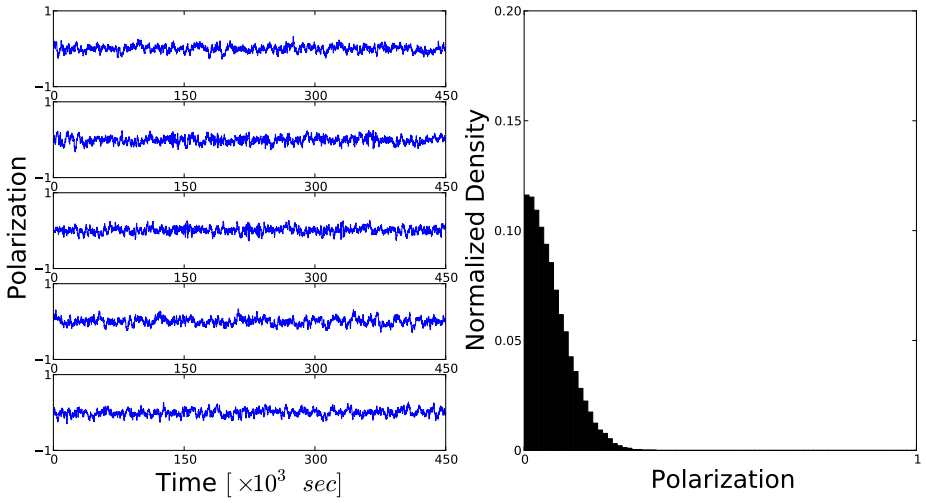

Figure 5.2: **Time-series of polarization with no interaction bias**. The polarization of the system is measured once every 50 seconds, and the resulting time-series of the polarization order parameter from five separate runs identical parameters are shown in the set of plots on the left. The absolute value of the polarization is tabulated in the histogram on the right side.

We can control the degree of polarization by varying the parameters θ_{along} and

$\theta_{against}$. To minimize changes to the total rate of induced catastrophes, we kept the sum of the two critical angles equal to our reference system described in 2.1:

$$\theta_{along} + \theta_{against} = 40^\circ + 40^\circ = 80^\circ \tag{5.3}$$

For the reference system with $\theta_{against} = 40^\circ$, the time-series of the polarization and distribution of the measured polarity are shown in Figure 5.3.

In our reference system, there is no microscopic bias that would cause the nematically ordered array to become polarized. The distribution of the polarization, as expected, is centered at zero. Even though the system never maintains a well defined degree of polarization, there is significant fluctuations in the polarity to account for the polarized systems observed by Eren et al. [15].

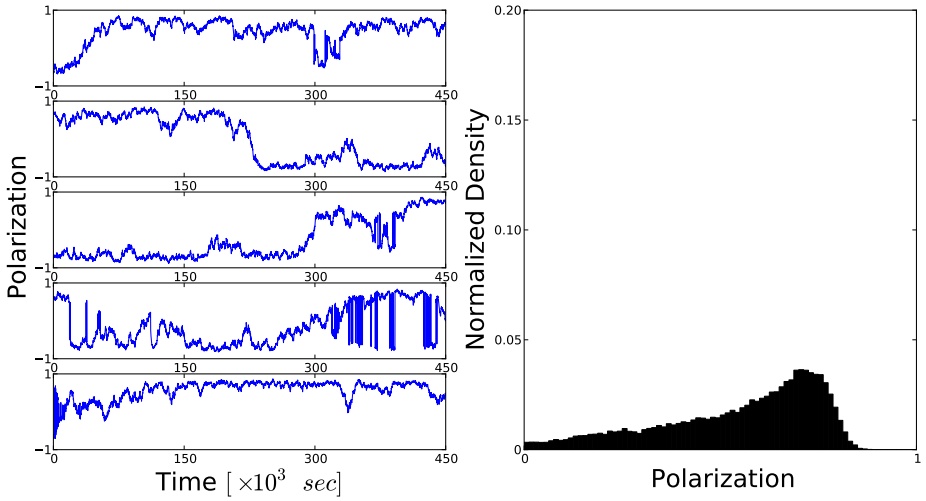

Figure 5.3: **Time-series of polarization with interaction bias**. Same as Figure 5.2. Showing the time-series and overall histogram of five runs are the with the same parameters with polarization bias: ($\theta_{along} = 70^\circ$ and $\theta_{against} = 10^\circ$)

To create systems with sustained polarity, we vary the degree of microscopic

polarization in the system (through θ_{againt} and θ_{along}). For small values of $\theta_{against}$ the system is capable of sustaining a non-zero polarization as shown in Figure 5.3. Since the sign of the polarity is only determined with respect to the orientation direction of the ordered CMT array, probability of observing a system with positive and negative polarizations are exactly equal. Hence, we only need to use the absolute value of the measured polarizations to study the phase behavior.

Note that for systems with measured polarization as small as 0.3, the corresponding nematically ordered array will have approximately 65% of the microtubules growing along the majority direction. The spread of the polarization distribution at zero bias is sufficient to account for the net polarization observed by Eren et al. [15]. In the systems with no interaction bias, CMT-dependent nucleation is the primary driver of the fluctuations in the measured polarization.

5.4 Phase transition of the polarization

As with the nematic ordering of cortical microtubule, we can gain a better understanding of the polar phase behavior through manipulation of the size of the simulated cell. Simulations are repeated five times at 40, 80, and 120 μm, for each system size, the interaction bias is controlled by the parameter $\theta_{against} = (40+6j)^\circ$ where $j = 0, 1, 2, 3, 4, 5$ and the restriction that $\theta_{along} + \theta_{against} = 80^\circ$. The absolute polarization of the system is measured at intervals of 50 seconds and resulting distributions are plotted separately for each system size in Figures 5.4

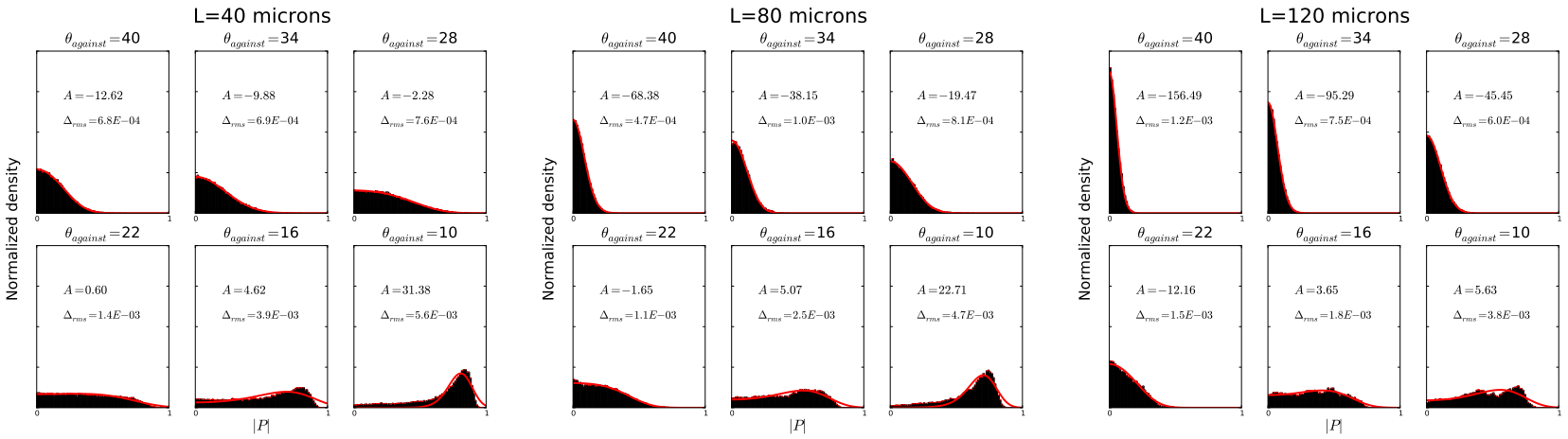

Figure 5.4: **Polar order distribution at different system sizes**. The the normalized distributions of the $|P|$ for systems of sizes $L = 40\,\mu m$, $L = 80\,\mu m$ and $L = 120\,\mu m$ the nematic order control parameter f_{gs}^{+} is fixed at the standar value of 0.006 for all runs. Each histogram represents the distribution of the order parameter value for five distinct runs. The distributions are fitted to quartic exponentials (shown in red) of the form $C\exp(Ax^2 + Bx^4)$. The fitting parameter A and root-mean-square difference between the data and the fit are given in each subplot.

The behavior of the absolute polarization order parameter closely resembles that of the nematic order parameter. For the smallest system size ($L = 40\,\mu m$), the absolute polarization has a broad distribution regardless of the degree of interaction bias in the simulated system.

As the size of the system is increased, the distribution becomes sharper for the completely unpolarized systems at $\theta_{against} = 40°$. A decrease in variance is not observed for the polarized system at $\theta_{against} = 10°$, this is likely due to the decrease in the nematic order. A slight downshift in the peak position is observed for the maximally polarized systems at $\theta_{against} = 10°$. Since the polarization of the CMT array is strongly dependent upon the underlying nematic organization, downshift in the polarization order parameter is tied to the similar downshift in the nematic order parameter discussed in the previous chapter.

The method of distinguishing nematically ordered and disordered states using the curvature of the fitting function can also be applied to the polarization order. Using the same fitting function — $C\exp(Ax^2 + Bx^4)$, we can again use the parameter A to indicate the curvature at $|P| = 0$. The computed values of the fitting parameter are plotted in Figure 5.5

Like the nematic transition, the polarization transition is difficult to identify. The polar order transition shares the same behavior of lower transition point as system size increases. As with the nematic order, the system shows a marked tendency to become disordered (negative values for A) at larger system sizes. The polarized system at $\theta_{against} = 10°$ showed progressively lower degrees of polarization as the system size is increased. The unpolarized systems were more sharply peaked about zero (indicated by a more negative fitting parameter), simply because the larger system size decreased the relative size of fluctuations. Using curvature

of the fitting function, we identify the transition from ordered to disordered phases to be in the range $\theta_{against} = 17^\circ \sim 22^\circ$. Since the polarization of the CMT array is established on top of nematically ordered systems, future studies should investigate how the polarization of the CMT array depends on the degree of nematic ordering in the system (controlled through the parameter f_{gs}^{+}).

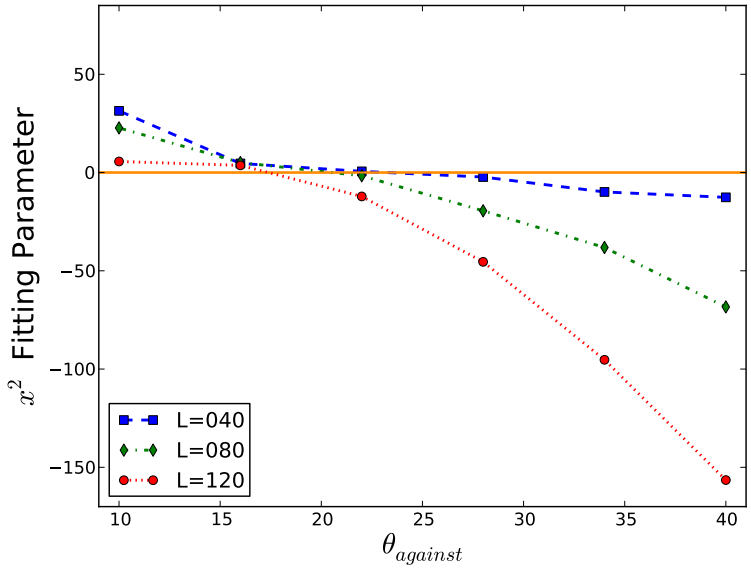

Figure 5.5: **Curvature of the polar fitting function.** The fitting parameter A (for the x^2 term in the exponential) is plotted against the control parameter $\theta_{against}$ for systems of size $L = 40\,\mu m$, $L = 80\,\mu m$, and $L = 120\,\mu m$ with $f_{gs}^{+} = 0.006$. The fitting parameter effectively defines the curvature of the histogram fitting function at the origin. If we identify the transition as the point where the fitting parameter curve crosses the $A = 0$ axis, we can see that the transition occurs at around $\theta_{against} = 17^\circ \sim 22^\circ$.

Chapter 6

Precession of CMT arrays

As we have seen in the previous chapters, changes in the microscopic behaviors of Cortical Microtubules have a profound effect on the macroscopic properties of the CMT array. Along with the nematic ordering and polarization discussed above, there are possible mechanisms for macroscopic chiral asymmetries originating from the inherent chiral structure of the microtubules themselves Ishida et al. [20], Thitamadee et al. [33]. An obvious manifestation of chiral asymmetry in our model is in the rotary motion of the CMT array.

Any single segment of CMT is assumed to be closely associated with the cortical membrane, thus prohibiting the translocation with respect to the membrane. The finite lifetime of the cortical microtubules allows for the nematic orientation angle Θ (as defined in Equation 4.4) to change over time.

Observation of rotary motion in developing CMT arrays was reported by Chan et al. [7], who showed that the CMT arrays in slowly growing *Arabidopsis* cells undergo reorientation. The patterns of reorientation differ greatly between cells, with some cells taking $200-800$ mins to complete one rotation of $360°$, while others never complete a full rotation. The direction of the rotation also differs between adjacent cells and may change in the same cell over time. The study also showed that the dynamic reorientation of the cortical array was arrested by the CMT-stabilizing drug Taxol, suggesting that microtubule dynamics is the driving force behind the reorientation.

In this chapter, we propose molecular mechanisms which allow the chiral structure of the microtubules to be translated into a handed asymmetry in the CMT-

depend nucleation or steep angle interactions between CMTs. Also, we demonstrate how the handed asymmetries will effects the reorientation of the macroscopic CMT arrays in our simulated systems.

6.1 Molecular mechanism

During the formation of individual microtubules polymers, the α and β tubulin dimers assemble into polarized linear protofilaments which forms weaker lateral bonds with neighboring protofilaments. The lateral interactions between tubulin dimers cause the protofilaments to form a closed tube, which is the final structure of the microtubule. Cryo-eletron microscopy of the basic structure of microtubules by Chrétien and Fuller [9], Li et al. [24] along with theoretical studies by Hunyadi et al. [19] revealed a persistent bias for the protofilaments to form "left-handed" microtubules, where the nearest α/β tubulin subunits form a left-handed helix along the length of the microtubule as illustrated in Figure 6.1 (Picture taken from [19] Figure 1). The offset between lateral dimers are fixed by the molecular structure of the tubulin subunits. Typically, the lateral interactions are between same type tubulin monomers, either $\alpha - \alpha$ or $\beta - \beta$. Since the typical microtubule consists of 13 to 14 protofilaments and the lateral offset is fixed, there is a "seam" along the length of the microtubule where the lateral interactions are of the weaker type, between α and β monomers, this seam is shown in orange in Figure 6.1.

While little is known regarding the exact molecular mechanism of cortical microtubule nucleation; CMT-dependent nucleation sites that facilitate the seeding of new microtubules are likely responsible for the seeding of microtubules in the cortex. Chan et al. [6] found evidence of recycling of nucleation sites, providing direct evidence for Mazia's hypothesis of a "flexible centrosome" in plants [25]. We

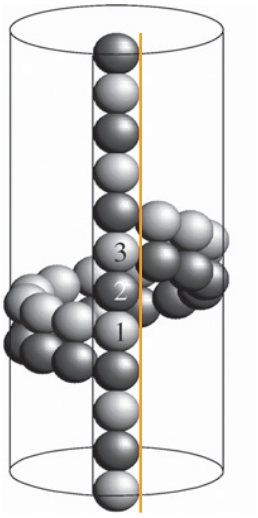

Figure 6.1: **Microtubule lattice configuration** of α/β tubulin heterodimers. The α and β tubulin subunits are represented by *dark* and *light* spheres respectively. Only one turn in the lateral helix and one protofiliment are shown. (Picture taken from [19] - Figure 1)

propose that a chiral nucleation complex that will bind to an existing "mother" CMT with a particular fixed handedness that is determined by the handedness of the CMT themselves. And since any nucleation complex of sufficient size would be sterically inhibited by interactions with the plasma membrane, we can expect that nucleation complex will always bind with the same orientation with respect to the polarity of the CMT and the normal to the plasm membrane. This fixed orientation allows for the introduction of a left-right asymmetry in the nucleation rate of the microtubules on either side of the mother CMTs.

Experimental study by Nakamura and Hashimoto [29] showed that a missense mutation, called *spiral3*, caused consistent oblique arrays with a fixed orientation along the elongation direction of the cell. The mutation causes a severe right-handed helical growth of epidermal cells.

The *spiral3* mutation causes the nucleation angle distribution to be wider and more divergent. But, since there is no reliable way of determining the growth direction of the mother CMT, angular distribution in this study did not distinguish between left and right side of the mother. We propose that the change in the angular distribution is due to a mutation affecting the probability of nucleation on either side of the mother CMT. This can be reproduced in our simulations by changing the rate of nucleation on both sides of the mother CMT, while keeping the total nucleation rate constant. The parameter that controls the probability of nucleating on the left side is called $\mathcal{P}_{left}$ — the ratio of CMT dependent nucleation that occurs on the left side of the mother CMT. The amount of CMT-dependent nucleation as a portion of all nucleation in the cortex is still fixed at 75 %.

Another possible molecular mechanism which is not accounted for in our current model is an interaction bias caused by the Brownian screw-ratchet mechanism described by Henley [18] and should result in the precession of the CMTs. This is due to the fact that addition of tubulin dimers onto the growing microtubule occurs in a left-handed helical pattern which creates an effective Brownian ratchet. Counting the +-end as the forward direction with the cell membrane above, this ratchet mechanism will tend to bend the incident CMT up into the membrane when it encounters a barrier CMT on the left side. In this case the Brownian screw will tend to bend the CMT up into the cell membrane which is energetically unfavorable due steric interactions. However, an encounter on the right side of the incident CMT will ratchet the incident CMT down (away from the plasma cell membrane). This creates an effective bias in the interaction between CMTs, specifically a difference in the cross-over and catastrophe probabilities.

The Brownian screw mechanism will cause a greater cross-over rate for inter-

actions where the barrier CMT is on the right side of the incident CMT (viewed from the other side of the cell membrane). This mechanism creates a rotational bias that will cause the system to rotate clockwise. The effects of the Brownian screw is not studied in this thesis, but should be included in futures studies with these simulations.

6.2 Control parameter

A convenient measure of the degree of nucleation coalignment was proposed by Deinum et al. [10], using the second cosine Fourier coefficient of the nucleation distribution:

$$\nu_2 = \int_{-\pi}^{\pi} d\theta \, \cos(2\theta) \, \nu(\theta) \tag{6.1}$$

Where $\nu(\theta)$ is the CMT-dependent nucleation distribution function. This parameter attains a maximal value of $\nu_2 = 1$ for completely collinear nucleation (either along or against the growth direction of the mother CMT), and a minimal value of $\nu_2 = -1$ for completely perpendicular nucleation.

Similarly, we can use the sine coefficient to measure the degree of left-right nucleation bias.

$$\eta_2 = \int_{-\pi}^{\pi} d\theta \, \sin(2\theta) \, \nu(\theta) \tag{6.2}$$

For CMTs that are nucleated parallel with the mother microtubule, no contribution will be made to rotation to either direction. Also, if the system has attained a high degree of nematic order, perpendicularly nucleated CMTs are more likely to be short lived due to encounters with catastrophe inducing barrier CMTs. Thus,

perpendicularly nucleated CMTs have very little effect on the reorientation of the CMT array. A positive value of η_2 indicates a bias for left handed rotation, and a negative value indicates a bias for right handed rotation.

For our simulations, the nucleation distribution is:

$$\nu(\theta) = \begin{cases} 0, & \text{if } |\theta| > 50^\circ \\ \left(\frac{180}{50\pi}\right), & \text{otherwise} \end{cases} \tag{6.3}$$

where we have converted the 50° range to $\frac{50\pi}{180}$ radians and normalized the nucleation probability on the range $[-\pi, \pi)$.

We can modify the nucleation distribution by changing only the probability of nucleating on either side of the mother CMT. We call the probability of nucleating on the left side (positive angular difference) of the mother microtubule $\mathcal{P}_{left}$, so the nucleation distribution becomes:

$$\nu(\theta) = \begin{cases} 0, & \text{if } |\theta| > 50^\circ \\ \left(\frac{180}{50\pi}\right)\mathcal{P}_{left}, & 0 < \theta < 50^\circ \\ \left(\frac{180}{50\pi}\right)(1 - \mathcal{P}_{left}), & 0 > \theta > -50^\circ \end{cases} \tag{6.4}$$

For the maximal nucleation angle of $\theta_{max} = 50^\circ$, we can obtain the second Fourier coefficient η_2 analytically, giving:

$$\eta_2 = \left(\frac{180}{100\pi}\right)(2\mathcal{P}_{left} - 1)\sin^2(\theta_{max}) \tag{6.5}$$

Estimation of the parameter η_2 can be made using the nucleation angle histograms from Chan et al. [8] — shown in Figure 6.2, which gives a values $\eta_2 = 0.183$.

Thus, changing the control parameter $\mathcal{P}_{left}$ will linearly vary the value of η_2. To illustrate the precession of a nematically ordered system we chose a specific value

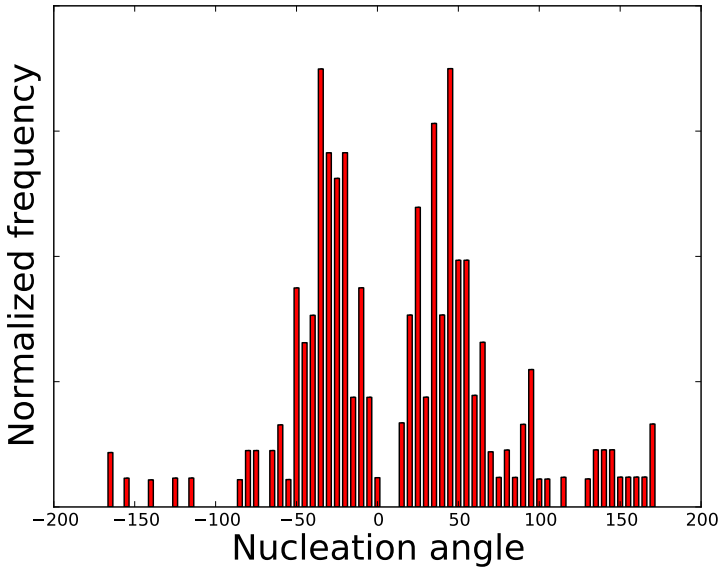

Figure 6.2: **Experimentally observed nucleation bias**. The observed nucleation distribution obtained from experiments is [8]. The distribution was digitized from the bar heights in Figure 2.C in [8]. The results were used to calculate the degree of nucleation bias (η_2) in the real CMT systems.

of the nucleation bias — $\mathcal{P}_{left} = 0.6$ and took snapshots of the system at intervals of $6,000$ seconds. The resulting system snapshots and the associated angle are shown in Figure 6.3.

In future studies, we will determine how effective the parameter $\eta_2 = \langle \sin(2\theta) \rangle$ is at predicting the rotary motion of CMT arrays.

6.3 Measuring rotation

Observations by Chan et al. [7] showed that rotary motion of CMTs occurs on the order of $0 \rightsquigarrow 2$ full rotations during a span of 8 hours. Assuming that the

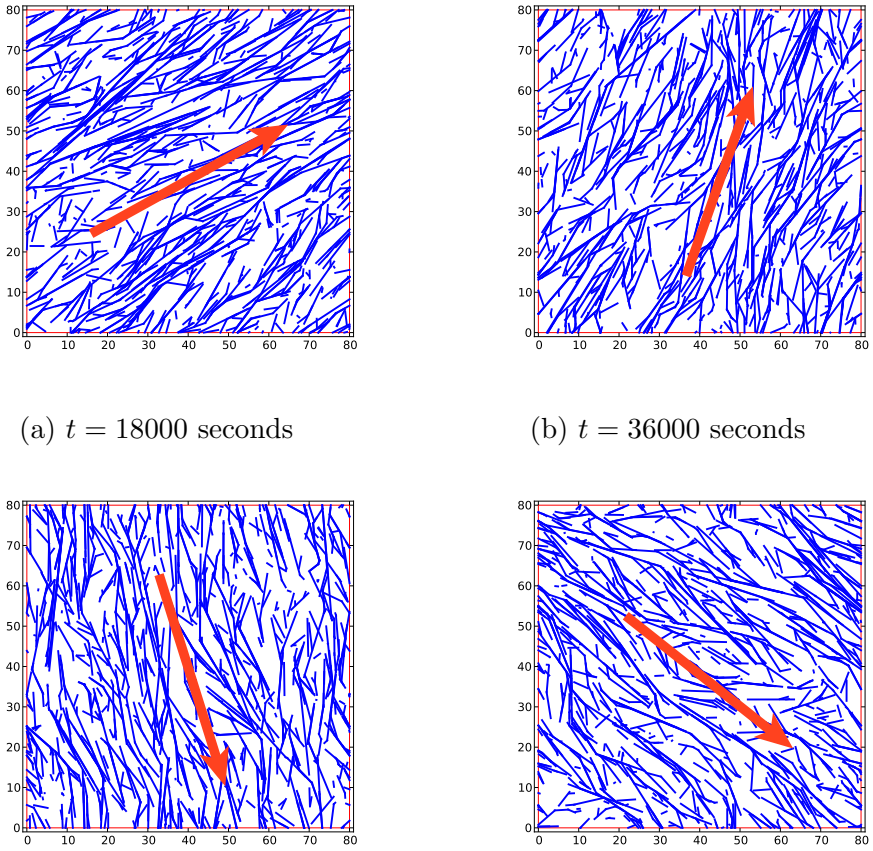

(a) $t = 18000$ seconds

(b) $t = 36000$ seconds

(c) $t = 54000$ seconds

(d) $t = 72000$ seconds

Figure 6.3: **Snapshots of a precessing system** with $\mathcal{P}_{left} = 0.6$. The snapshots are taken with an interval of $6,000$ seconds starting after a period of $18,000$ seconds to allow the nematic order to be fully established. Note that the arrow indicating the nematic array orientation angle Θ always point to the right because the angle is only defined on a range of $\left[-\frac{\pi}{2}, \frac{\pi}{2}\right)$ as given in Equation 4.4.

average number of rotations is ≈ 1 we obtain an approximate rotation rate of $2.2^{-4}\, radians/sec$. The rates of CMT array precession will depend on both the degree of left-right asymmetry that is causing the rotation and the dynamicity of the CMTs in the system which governs robustness of the established nematic order.

Since changes in the dynamicity are typically gradual and our standard system parameter set is in a regime of higher order, the nematic order will not change appreciably without dramatically altering the dynamicity of the individual CMTs. We choose to fix the dynamicity parameters at the standard values, and only vary the degree of asymmetry through the control parameter $\mathcal{P}_{left}$.

As we have shown in Figure 4.2, the array orientation angle has a tendency to be in found at $\Theta = 0$, *or* $\pm \frac{\pi}{2}$, due to the nematically organized array interacting with itself across the periodic boundaries of the system. However, the effect of this locking is not significant, as angular precession of the array angle Θ does not dwell significantly at the preferential angles for any of the nucleation biased systems with $\mathcal{P}_{left} \neq 0.5$ examined in this report.

Given that the array orientation angle Θ is only defined within multiples of π and the fact that the orientation angle fluctuates dramatically before the nematic ordering is established, the absolute rotation of the CMT array is not readily identified. We define the relative rotation of our system with respect to its orientation after an initialization time of 1000 sampling intervals (with a sampling period of $50\, sec$). Since nematic order is well established by this time, the changes in the orientation angle is solely due to the left-right bias we introduced to the system.

By stipulating that system cannot rotate by 180° during one sampling period, we can wrap the measured orientation angles in one continuous time series. The

orientation angle time series for various values of the control parameter $\mathcal{P}_{left}$ is shown in Figure 6.4.

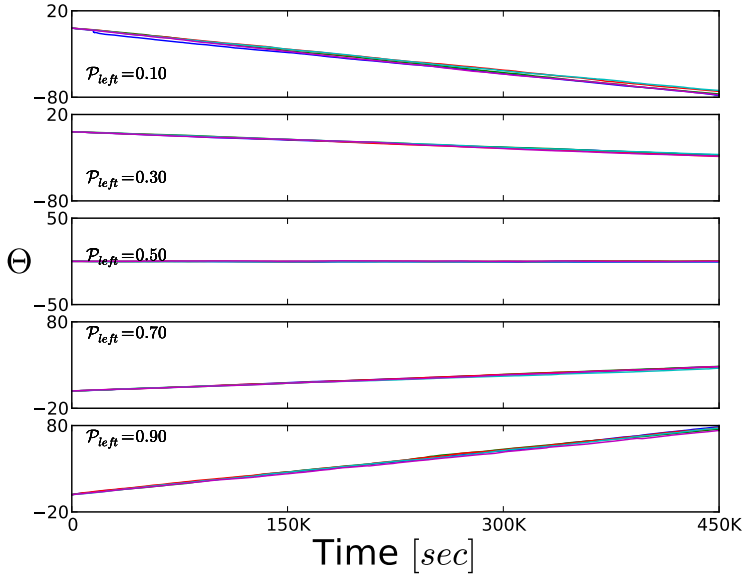

Figure 6.4: **Array orientation time-series**. Measurements of the relative array orientation angle with respect to orientation angle at $50,000\,sec$. Each subplot shows the time series from five distinct runs [shown in different colors] with all with $f_{gs}^{+} = 0.006$ and $k_n = 0.001$. Between subplots, the value of the nucleation bias control parameter $\mathcal{P}_{left}$ is varies in equal steps from 0.1 to 0.9.

The angular velocity can be computed for each individual run by dividing the final angular displacement by the total time of 4.5×10^5 seconds. The resulting angular velocities for all five individual runs are plotted against the nucleation bias parameter η_2 (which can be computed using Equation 6.1) and shown in Figure 6.5, along with the mean and standard deviation indicated by the red error bars.

The measured rate of CMT array reorientation are similar to the rates reported by Chan et al. [7]. The digitally extracted value from the histogram in Figure 6.2

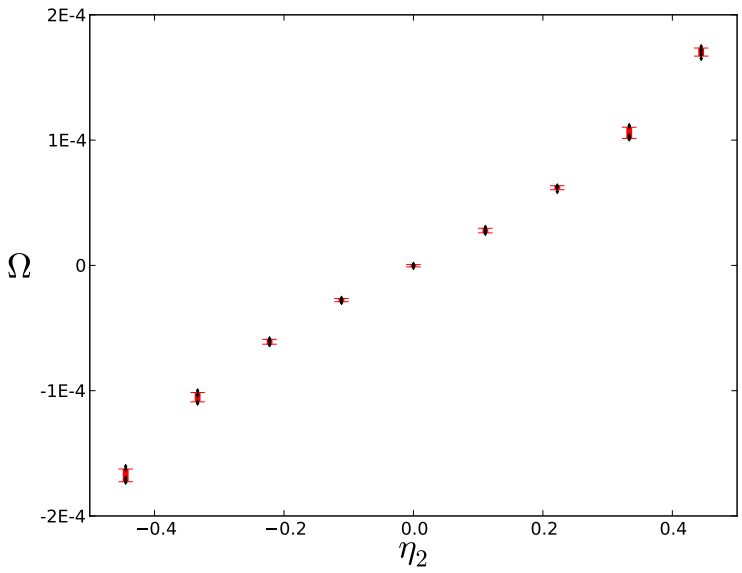

Figure 6.5: **Angular velocity vs. nucleation bias**. The average angular velocity of each five independent runs were computed and plotted (black dots) for $\mathcal{P}_{left}$ values ranging from 0.1 to 0.9. The x-axis represents the converted η_2 values calculated from $\mathcal{P}_{left}$, and the y-axis represents the measured rates of array precession.

gives $\eta_2 = 0.183$, which gives the linearly interpolated precession rate of $\Omega = 4.99 \times 10^{-5}\, rad/sec$, within an order of magnitude of the observed value: $2.2 \times 10^{-4}\, rad/sec$ from experiments [7]. As suggested in Chapter 4 for the polarization order, future studies should investigate how the nematic ordering of the CMT arrays can quantitatively affect the precession rates of the orientation angle since the angle is only defined for nematically ordered arrays.

Chapter 7

CONCLUSION AND FUTURE OUTLOOK

In this thesis, we have addressed some important aspects of the present understanding of cortical microtubule array organization. Namely, the polarization and reorientation of nematically organized arrays. We also developed a better understanding of the nematic order transition by looking at the fluctuations of the order parameters for long periods of time. Important findings in the course of theses studies are highlighted in the following sections.

7.1 Sustained macroscopic asymmetries

7.1.1 Polarization of CMT arrays

The direction independent nematic organization of CMT arrays have been well documented in previous studies [2] [15] [10], but the development of sustained polar organization in these arrays have largely been neglected. Eren et al. [15] showed that it is not possible to attain a high degree of CMT polarity with only CMT-independent nucleation in the cortical media between the CMTs. With the inclusion of CMT-dependent nucleation in the simulations, the probability of observing a net polarity was significantly higher. However, there were no evidence of sustained polarization in the system as the system continues to evolve in time.

In Chapter 5 we proposed a model for asymmetric interactions between copolar and antipolar CMTs that resulted in different effective entrainment rates for the two different situations. To measure the degree of polarization in the system, we use

an order parameter given by the projection of the length-weighted average growth direction onto a unit vector along the array orientation angle. If we incorporate CMT-dependent nucleation in the simulations, we observed a broad distribution of the polar order parameter with sufficiently large fluctuations that accounts for the polarized snapshots found by [15]. However, the distribution is still centered at zero, which means on average, the system is not polarized. Once the asymmetric interactions are included in the simulations, the systems are able maintain a certain degree of polarization, and the order parameter will be peaked at a non-zero value.

7.1.2 Precession of CMT arrays

A possible mechanism of left-right nucleation bias was presented in Chapter 6. The macroscopic precession rate of the CMT array is given by the angular velocity of the drift in the array orientation angle. It was noted by Deinum et al. [10] that the small percentage of nucleation bias reported by Chan et al. [8] was insufficient in creating sufficient precession in the CMT array. However, in the case of CMT-dependent nucleation, if we characterize the degree of nucleation bias by the second Fourier coefficient instead the nucleation probability on either side of the mother CMT, the scale of the nucleation bias is commensurate with the degree of nucleation bias reported in [8]. The precession rates also agree well with the experimentally observed rotation reported in [7].

7.2 Method for measuring orders

The core results of this thesis are for the measurement of three global properties (nematic order, polarization order, and array precession) and in each case we discussed the existing thoughts and developed a method to measure it.

The nematic organization of CMT arrays has been well established in previous studies [2][15][10]. Using only the ensemble average of the scalar order parameter S_2 (Equation 4.3) as a measure of orientational order is useful for distinguishing strongly ordered or disordered systems, but ineffective in describing the organization of intermediate systems around where the transition from order disorder occurs. Using the distribution of S_2 values, we can identify a system as nematically disordered if the distribution attains a maximal value at the origin, and nematically ordered if the maxima is elsewhere. To quench the statistical fluctuations inherent in such simulations, we fitted the recorded distribution to a quartic exponential of the form (Equation 4.5). The parameter A is directly related to the curvature of the distribution at the point $S_2 = 0$ — a positive A value indicates a *minima* while a negative A value indicates a *maxima*. Using the definition of the transition and control parameters k_n and f_{gs}^{+}, we were able to produce a rough description of the phase space and its dependence on the size of the system.

Even though the system can have local order, the correlation decreases as the system size gets bigger so global order cannot be achieved. We have shown that the ensemble average of the order parameter is not an intrinsic property of the set of dynamics parameter governing the growth and interaction of the CMT arrays, but an artifact of the finite size of the system we are simulating. As we have shown in Chapter 4, the measured order parameter is also strongly dependent on the size of the system. So a more detailed study of the parametrization of the orientational order is required.

For the polarization order studies in Chapter 5, we employed the same method of analysis to the polarization order parameter $|P|$ and the control parameter $\theta_{against}$. Using the curvature at the origin where $|P| = 0$, we identify the tran-

sition point again as the point where the curvature of the fitting function of the time-domain distribution is zero at the origin. The control parameter $\theta_{against}$ determines the interaction bias between copolar and antipolar CMTs. We find that the inclusion of CMT-dependent nucleation alone ($\theta_{against} = \theta_c$) is not enough to produce a sustained polarity in the array, but larger degrees of interaction bias were sufficient. We also noted that the transition point moved towards higher polarization bias (lower $\theta_{against}$ value) as the system size increased.

The precession of the CMT array does not lend itself to the same type of order parameter analysis we have done above. To investigate the precession behavior in Chapter 6 we studied the array precession rate with the control parameter $|\mathcal{P}|$ — which determines the bias of nucleating on the left and right side of the CMT. The result where in rough agreement with the experimentally observed nucleation bias and precession rate reported in the literature.

7.3 Future outlook

The microscopic asymmetries that gave rise to the macroscopic polarization and precession behavior, suggests specific types of molecular mechanism responsible for the behavior. The results of our simulation suggests that the polarization properties of the CMT array could be explained by the existence of protein linkers similar to the MAP65 linker protein with an affinity to bundle copolar CMTs. If such a protein were found, one can conceivably control the degree of polarization within the CMT arrays by modulating the availability of such a linker protein. The precession of the CMT array suggests possible asymmetries in the CMT nucleating complex and provides further motivation to determine their exact molecular structure. As with any other phenomenological prediction of bio-molecular properties,

we should only use the predictions as a rough guide since our understanding of the molecular processes inside the cell is still lacking.

In future studies, we can use the simulations we built and the analytical techniques we developed to probe more aspects of the macroscopic symmetry breaking. For the nematic ordering of CMT arrays, a more comprehensive survey of the k_n/f_{gs}^+ phase space can be done and compared to the results from [32] where only steric interactions where included in the simulations. For the precession of CMT arrays, we can test the robustness of the nucleation bias parameterization η_2 from Equation 6.2 with a set of different nucleation distributions. In addition, we can include other interaction biases into the simulation, such as a more favorable cross-over due to the thermal ratcheting of incident CMTs (discussed in Section 6.1), which serves as another source of rotational bias in the system.

Chapter 8

Acknowledgments

First and formost, I would like to extend my deepest gratitude to my research supervisor Professor Christopher Henley, for his patient guidance and helpful critiques during the course of this project. I am also grateful for the help of Ricky Chachra, especially his assistance in my orientation to both bio-physics research and the computational tools that I would need, as well as his continued contribution in weekly discussions with Professor Henley and myself. I would also like to thank Igor Segota for his work on the early versions of the microtubule simulation code.

BIBLIOGRAPHY

[1] Jun F. Allard, J. Christian Ambrose, Geoffrey O. Wasteneys, and Eric N. Cytrynbaum. A Mechanochemical Model Explains Interactions between Cortical Microtubules in Plants. *Biophysical Journal*, 99(4):1082–1090, August 2010. ISSN 00063495. doi: 10.1016/j.bpj.2010.05.037. URL http://dx.doi.org/10.1016/j.bpj.2010.05.037.

[2] Jun F. Allard, Geoffrey O. Wasteneys, and Eric N. Cytrynbaum. Mechanisms of Self-Organization of Cortical Microtubules in Plants Revealed by Computational Simulations. *Molecular Biology of the Cell*, 21(2):278–286, January 2010. ISSN 1939-4586. doi: 10.1091/mbc.e09-07-0579. URL http://dx.doi.org/10.1091/mbc.e09-07-0579.

[3] J. Christian Ambrose and Geoffrey O. Wasteneys. CLASP Modulates Microtubule-Cortex Interaction during Self-Organization of Acentrosomal Microtubules. *Molecular Biology of the Cell*, 19(11):4730–4737, November 2008. ISSN 1939-4586. doi: 10.1091/mbc.e08-06-0665. URL http://dx.doi.org/10.1091/mbc.e08-06-0665.

[4] James L. Antonakos and Kenneth C. Mansfield. *Practical Data Structures Using C/C++*. Prentice Hall, 1st edition, January 1999. ISBN 013026864X. URL http://www.worldcat.org/isbn/013026864X.

[5] Jordi Chan, Cynthia G. Jensen, Lawrence C. W. Jensen, Max Bush, and Clive W. Lloyd. The 65-kDa carrot microtubule-associated protein forms regularly arranged filamentous cross-bridges between microtubules. *Proceedings of the National Academy of Sciences*, 96(26):14931–14936, December 1999. ISSN 1091-6490. doi: 10.1073/pnas.96.26.14931. URL http://dx.doi.org/10.1073/pnas.96.26.14931.

[6] Jordi Chan, Grant M. Calder, John H. Doonan, and Clive W. Lloyd. EB1 reveals mobile microtubule nucleation sites in Arabidopsis. *Nature cell biology*, 5(11):967–971, November 2003. ISSN 1465-7392. doi: 10.1038/ncb1057. URL http://dx.doi.org/10.1038/ncb1057.

[7] Jordi Chan, Grant Calder, Samantha Fox, and Clive Lloyd. Cortical microtubule arrays undergo rotary movements in Arabidopsis hypocotyl epidermal cells. *Nat Cell Biol*, 9(2):171–175, February 2007. ISSN 1465-7392. doi: 10.1038/ncb1533. URL http://dx.doi.org/10.1038/ncb1533.

[8] Jordi Chan, Adrian Sambade, Grant Calder, and Clive Lloyd. Arabidopsis Cortical Microtubules Are Initiated along, as Well as Branching from, Existing Microtubules. *The Plant Cell Online*, 21(8):2298–2306, August 2009. ISSN 1532-298X. doi: 10.1105/tpc.109.069716. URL http://dx.doi.org/10.1105/tpc.109.069716.

[9] D. Chrétien and S. D. Fuller. Microtubules switch occasionally into unfavorable configurations during elongation. *Journal of molecular biology*, 298 (4):663–676, May 2000. ISSN 0022-2836. doi: 10.1006/jmbi.2000.3696. URL http://dx.doi.org/10.1006/jmbi.2000.3696.

[10] Eva E. Deinum, Simon H. Tindemans, and Bela M. Mulder. Taking directions: the role of microtubule-bound nucleation in the self-organization of the plant cortical array. *Physical biology*, 8(5), October 2011. ISSN 1478-3975. doi: 10.1088/1478-3975/8/5/056002. URL http://dx.doi.org/10.1088/1478-3975/8/5/056002.

[11] Ram Dixit and Richard Cyr. Encounters between Dynamic Cortical Microtubules Promote Ordering of the Cortical Array through Angle-Dependent Modifications of Microtubule Behavior. *The Plant Cell Online*, 16(12):3274–3284, December 2004. ISSN 1532-298X. doi: 10.1105/tpc.104.026930. URL http://dx.doi.org/10.1105/tpc.104.026930.

[12] Ram Dixit, Eric Chang, and Richard Cyr. Establishment of Polarity during Organization of the Acentrosomal Plant Cortical Microtubule Array. *Molecular Biology of the Cell*, 17(3):1298–1305, March 2006. ISSN 1939-4586. doi: 10.1091/mbc.e05-09-0864. URL http://dx.doi.org/10.1091/mbc.e05-09-0864.

[13] Marileen Dogterom and Stanislas Leibler. Physical aspects of the growth and regulation of microtubule structures. *Physical Review Letters*, 70:1347–1350, March 1993. doi: 10.1103/physrevlett.70.1347. URL http://dx.doi.org/10.1103/physrevlett.70.1347.

[14] David W. Ehrhardt and Sidney L. Shaw. Microtubule dynamics and organization in the plant cortical array. *Annual review of plant biology*, 57:859–875, 2006. ISSN 1543-5008. doi: 10.1146/annurev.arplant.57.032905.105329. URL http://dx.doi.org/10.1146/annurev.arplant.57.032905.105329.

[15] Ezgi C. Eren, Ram Dixit, and Natarajan Gautam. A Three-Dimensional Computer Simulation Model Reveals the Mechanisms for Self-Organization of Plant Cortical Microtubules into Oblique Arrays. *Molecular Biology of the Cell*, 21(15):2674–2684, August 2010. ISSN 1939-4586. doi: 10.1091/mbc.e10-02-0136. URL http://dx.doi.org/10.1091/mbc.e10-02-0136.

[16] Jérémie Gaillard, Emmanuelle Neumann, Daniel Van Damme, Virginie Stoppin-Mellet, Christine Ebel, Elodie Barbier, Danny Geelen, and Marylin Vantard. Two Microtubule-associated Proteins of Arabidopsis MAP65s Promote Antiparallel Microtubule Bundling. *Molecular Biology of the Cell*, 19 (10):4534–4544, October 2008. ISSN 1939-4586. doi: 10.1091/mbc.e08-04-0341. URL http://dx.doi.org/10.1091/mbc.e08-04-0341.

[17] Rhoda J. Hawkins, Simon H. Tindemans, and Bela M. Mulder. Model for the orientational ordering of the plant microtubule cortical array. *Physical Review E*, 82:011911+, July 2010. doi: 10.1103/physreve.82.011911. URL http://dx.doi.org/10.1103/physreve.82.011911.

[18] ChristopherL Henley. Possible Origins of Macroscopic Left-Right Asymmetry in Organisms. *Journal of Statistical Physics*, 148(4):740–774, June 2012. ISSN 0022-4715. doi: 10.1007/s10955-012-0520-z. URL http://dx.doi.org/10.1007/s10955-012-0520-z.

[19] Viktória Hunyadi, Denis Chrétien, Henrik Flyvbjerg, and Imre M. Jánosi. Why is the microtubule lattice helical? *Biology of the Cell*, 99(2):117–128, 2007. doi: 10.1042/bc20060059. URL http://dx.doi.org/10.1042/bc20060059.

[20] Takashi Ishida, Yayoi Kaneko, Megumi Iwano, and Takashi Hashimoto. Helical microtubule arrays in a collection of twisting tubulin mutants of Arabidopsis thaliana. *Proceedings of the National Academy of Sciences of the United States of America*, 104(20):8544–8549, May 2007. ISSN 0027-8424. doi: 10.1073/pnas.0701224104. URL http://dx.doi.org/10.1073/pnas.0701224104.

[21] Eiko Kawamura and Geoffrey O. Wasteneys. MOR1, the Arabidopsis thaliana homologue of Xenopus MAP215, promotes rapid growth and shrinkage, and suppresses the pausing of microtubules in vivo. *Journal of cell science*, 121 (Pt 24):4114–4123, December 2008. ISSN 0021-9533. doi: 10.1242/jcs.039065. URL http://dx.doi.org/10.1242/jcs.039065.

[22] Yulia A. Komarova, Ivan A. Vorobjev, and Gary G. Borisy. Life cycle of MTs: persistent growth in the cell interior, asymmetric transition frequencies and effects of the cell boundary. *Journal of cell science*, 115(Pt 17):3527–3539, September 2002. ISSN 0021-9533. URL http://jcs.biologists.org/cgi/content/abstract/115/17/3527.

[23] M. C. Ledbetter and K. R. Porter. A "microtubule" in plant cell fine structure. *The Journal of Cell Biology*, 19(1):239–250, October 1963. ISSN 1540-8140. doi: 10.1083/jcb.19.1.239. URL http://dx.doi.org/10.1083/jcb.19.1.239.

[24] Huilin Li, David J. DeRosier, William V. Nicholson, Eva Nogales, and Kenneth H. Downing. Microtubule structure at 8 A resolution. *Structure (London, England : 1993)*, 10(10):1317–1328, October 2002. ISSN 0969-2126. URL http://view.ncbi.nlm.nih.gov/pubmed/12377118.

[25] D. Mazia. Centrosomes and mitotic poles. *Experimental cell research*, 153(1):1–15, July 1984. ISSN 0014-4827. URL http://view.ncbi.nlm.nih.gov/pubmed/6734733.

[26] N. D. Mermin and H. Wagner. Absence of Ferromagnetism or Antiferromagnetism in One- or Two-Dimensional Isotropic Heisenberg Models. *Physical Review Letters*, 17(22):1133–1136, November 1966. doi: 10.1103/physrevlett.17.1133. URL http://dx.doi.org/10.1103/physrevlett.17.1133.

[27] Tim Mitchison and Marc Kirschner. Dynamic instability of microtubule growth. *Nature*, 312(5991):237–242, November 1984. doi: 10.1038/312237a0. URL http://dx.doi.org/10.1038/312237a0.

[28] Takashi Murata, Seiji Sonobe, Tobias I. Baskin, Susumu Hyodo, Seiichiro Hasezawa, Toshiyuki Nagata, Tetsuya Horio, and Mitsuyasu Hasebe. Microtubule-dependent microtubule nucleation based on recruitment of [gamma]-tubulin in higher plants. *Nat Cell Biol*, 7(10):961–968, October 2005. ISSN 1465-7392. doi: 10.1038/ncb1306. URL http://dx.doi.org/10.1038/ncb1306.

[29] Masayoshi Nakamura and Takashi Hashimoto. A mutation in the Arabidopsis -tubulin-containing complex causes helical growth and abnormal microtubule branching. *Journal of Cell Science*, 122(13):2208–2217, July 2009. ISSN 1477-9137. doi: 10.1242/jcs.044131. URL http://dx.doi.org/10.1242/jcs.044131.

[30] Peter Olsson. Monte carlo analysis of the two-dimensional XY model. ii. comparison with the kosterlitz renormalization-group equations. *Physical Review B*, 52:4526–4535, August 1995. doi: 10.1103/physrevb.52.4526. URL http://dx.doi.org/10.1103/physrevb.52.4526.

[31] Sidney L. Shaw, Roheena Kamyar, and David W. Ehrhardt. Sustained Microtubule Treadmilling in Arabidopsis Cortical Arrays. *Science*, 300(5626):1715–1718, June 2003. ISSN 1095-9203. doi: 10.1126/science.1083529. URL http://dx.doi.org/10.1126/science.1083529.

[32] Xia-qing Shi and Yu-qiang Ma. Understanding phase behavior of plant cell cortex microtubule organization. *Proceedings of the National Academy of Sciences*, 107(26):11709–11714, June 2010. ISSN 1091-6490. doi: 10.1073/pnas.1007138107. URL http://dx.doi.org/10.1073/pnas.1007138107.

[33] Siripong Thitamadee, Kazuko Tuchihara, and Takashi Hashimoto. Microtubule basis for left-handed helical growth in Arabidopsis. *Nature*, 417(6885):193–196, May 2002. doi: 10.1038/417193a. URL http://dx.doi.org/10.1038/417193a.

[34] Simon H. Tindemans, Rhoda J. Hawkins, and Bela M. Mulder. Survival of the Aligned: Ordering of the Plant Cortical Microtubule Array. *Physical Review Letters*, 104(5):058103+, February 2010. doi: 10.1103/physrevlett.104.058103. URL http://dx.doi.org/10.1103/physrevlett.104.058103.

[35] Jan W. Vos, Marileen Dogterom, and Anne M. Emons. Microtubules become more dynamic but not shorter during preprophase band formation: A possible search-and-capture mechanism for microtubule translocation. *Cell Motil. Cytoskeleton*, 57(4):246–258, April 2004. ISSN 0886-1544. doi: 10.1002/cm.10169. URL `http://dx.doi.org/10.1002/cm.10169`.

[36] Geoffrey O. Wasteneys and J. Christian Ambrose. Spatial organization of plant cortical microtubules: close encounters of the 2D kind. *Trends Cell Biol*, 19(2):62–71, February 2009. ISSN 09628924. doi: 10.1016/j.tcb.2008.11.004. URL `http://dx.doi.org/10.1016/j.tcb.2008.11.004`.

[37] Geoffrey O. Wasteneys and Richard E. Williamson. Reassembly of microtubules in Nitella tasmanica: assembly of cortical microtubules in branching clusters and its relevance to steady-state microtubule assembly. *Journal of Cell Science*, 93(4):705–714, August 1989. ISSN 1477-9137. URL `http://jcs.biologists.org/content/93/4/705.abstract`.

[38] Raymond Wightman and Simon R. Turner. Severing at sites of microtubule crossover contributes to microtubule alignment in cortical arrays. *The Plant journal : for cell and molecular biology*, 52(4):742–751, November 2007. ISSN 0960-7412. doi: 10.1111/j.1365-313x.2007.03271.x. URL `http://dx.doi.org/10.1111/j.1365-313x.2007.03271.x`.